Investigating the Interactions Between PI4KA and its Accessory Proteins

Mackenzie K. Scott

Thesis submitted to
The Department of Biochemistry and Microbiology
In partial fulfillment of the requirements for
Bachelor of Science (Hons.)

University of Victoria
Victoria, British Columbia, Canada
April 2023

Abstract

Phosphoinositides are important signaling molecules within all eukaryotic cells and are involved in essential processes such as cell growth and metabolism. Phosphatidylinositol 4-phosphate (PI4P) is one of the most abundant species of phosphoinositides in mammalian cells, and can be produced by phosphoinositide 4-kinases (PI4Ks). Phosphoinositide 4-kinase IIIα (PI4KA) is responsible for generating pools of PI4P at the plasma membrane, which is essential for lipid exchange and plasma membrane asymmetry. It has been established that PI4KA associates with the regulatory proteins TTC7 and FAM126, however the exact mechanisms behind the recruitment of the PI4KA regulatory complex to the plasma membrane are not well understood at the molecular level. The putative mechanism of recruitment involves the membrane protein EFR3, whose C-terminus interacts with TTC7 and FAM126 on the PI4KA regulatory complex. To investigate the interaction between EFR3 and TTC7/FAM126, a construct containing full length TTC7B and truncated FAM126A (2-308) was designed, as well as a construct containing the C-terminal residues of EFR3A (721-791). Using an AlphaFold model as a guide, mutations were designed at the putative EFR3A (721-791)/TTC7B/FAM126A (2-308) binding interface. Biolayer interferometry was used to measure the affinity between wild type EFR3A (721-791) and TTC7B/FAM126A (2-308), and to compare the binding affinity between various mutants. Of the mutants generated, F755A, L731A, and I763A of EFR3A showed a large reduction in response when compared to the wild type. Our results reveal a partial structure of the EFR3A (721-791)/TTC7B/FAM126A (2-308) binding interface, and how key amino acids mediate this interaction.

Table of Contents

List of Figures

List of Tables

List of Abbreviations

Akt – A serine/threonine protein kinase
bME – β-mercaptoethanol
BLI – Biolayer interferometry
EDTA – Ethylenediaminetetraacetic acid
EFR3 – Membrane protein
ER – Endoplasmic reticulum
FAM126 – Hyccin
GFB – Gel filtration buffer
HCV – Hepatitis C virus
HEPES – 4-(2-hydroxyethyl)-1-piperazineethanesulfonic acid
KD – Dissociation constant
PC – Phosphatidylcholine
PE – Phosphatidylethanolamine
PI – Phosphatidylinositol
PI4K – Phosphatidylinositol 4-kinase
PI4KA – Phosphatidylinositol 4-kinase IIIα
PI4KB – Phosphatidylinositol 4-kinase IIIβ
PI4P – Phosphatidylinositol 4-phosphate
PIP_2 – Phosphatidylinositol 4,5 bisphosphate
PIP_3 – Phosphatidylinositol 3,4,5 trisphosphate
PM – Plasma membrane
PS – Phosphatidylserine
NiNTA – Nickel nitriloacetic acid
SEC – Size exclusion chromatography
Stt4 – Yeast homolog of PI4KA
TCEP – Tris(2-carboxyethyl)phosphine
TEV – Tobacco etch virus
TTC7 – Tetratricopeptide repeat domain 7
Ypp1 – Yeast homolog of TTC7

Acknowledgements

First and foremost, I would like to thank Dr. John Burke for the opportunity to work and study in the lab, and for his guidance along the way. It's been an incredible experience, and I cannot believe how quickly the time has flown by. Looking back, the progress I've made in every aspect of my career as a scientist was astronomical, and I'm so excited to continue learning with everyone. Furthermore, this project would not have been possible without the tremendous effort invested by Sushant Suresh, who guided me every step of the way and was more than happy to answer every question I had (even if it was the tenth time I asked it). I cannot believe I didn't find the limit to Sushant's patience; it's not like I didn't try. Meredith Jenkins was also a vital part of this project, and always provided crucial advice at key moments to make sure I didn't destroy the equipment. Thank you also to Alex Shaw, who managed to make a scientific writer out of me, as well as Isobel Barlow-Busch, Noah Harris, Matthew Parson(s), and John Evans for their advice along the way.

I'd also like to thank my family, especially my mum and dad, as well as my friends, teammates, and coaches for dealing with my hectic life these past eight months. Their support throughout this time was just as important as all the science that went into this project, and it would not have been possible without their never-ending encouragement.

Introduction

Phospholipids and Cell Membranes

The proper structure and function of all eukaryotic cells is dependent on cellular membranes, which are essential for separating individual cells from the rest of their environment and defining intracellular compartments, such as the nucleus and other cytoplasmic organelles. These membranes consist of specific proteins and bilayers of phospholipids; examples include phosphatidylserine (PS), phosphatidylcholine (PC), phosphatidylethanolamine (PE), and phosphatidylinositol (PI) (van Meer et al., 2008). All phospholipids are amphiphilic: they contain a hydrophilic head group, which includes a phosphate group bound to a glycerol backbone, and can have different overall charges. The headgroup is linked to two hydrophobic hydrocarbon tails, which vary in their length and saturation (Li et al., 2015). The nature of these lipids allows them to form bilayers spontaneously in aqueous environments, making the bilayer an ideal structure for cell membranes.

Not only are phospholipids of essential structural importance, but they also serve as important signaling molecules. Notably, phosphoinositides are important regulators of cellular signaling, and are involved in essential processes such as cell growth and metabolism through regulation of processes such as vesicular transport and lipid distribution (Chung et al., 2015; D'Angelo et al., 2013). Phosphoinositides are well suited to cellular signaling because they can be reversibly phosphorylated at three different hydroxyl positions. Their diversity and specificity is critical for the proper regulation of eukaryotic cells, and as such the study of these lipids is vital to the understanding of important intracellular processes (G. R. Hammond & Burke, 2020).

Phosphoinositides and Cell Signaling

There are a total of seven different species of phosphoinositides, all of which are generated from PI by phosphorylation or dephosphorylation of the 3′, 4′, and 5′ positions on the inositol headgroup by specific kinases and phosphatases, respectively. Each species has specific subcellular localizations, as shown in figure 1. They are usually concentrated on the cytoplasmic side of cellular membranes, as an integral part of the lipid bilayer. The correct localization of each phosphoinositide species is fundamental to maintaining organelle identity and membrane trafficking, as membrane-cytosol interactions are determined by the heterogeneous subcellular localization of specific phosphoinositide species (Chang-Ileto et al., 2012; Di Paolo & De Camilli, 2006).

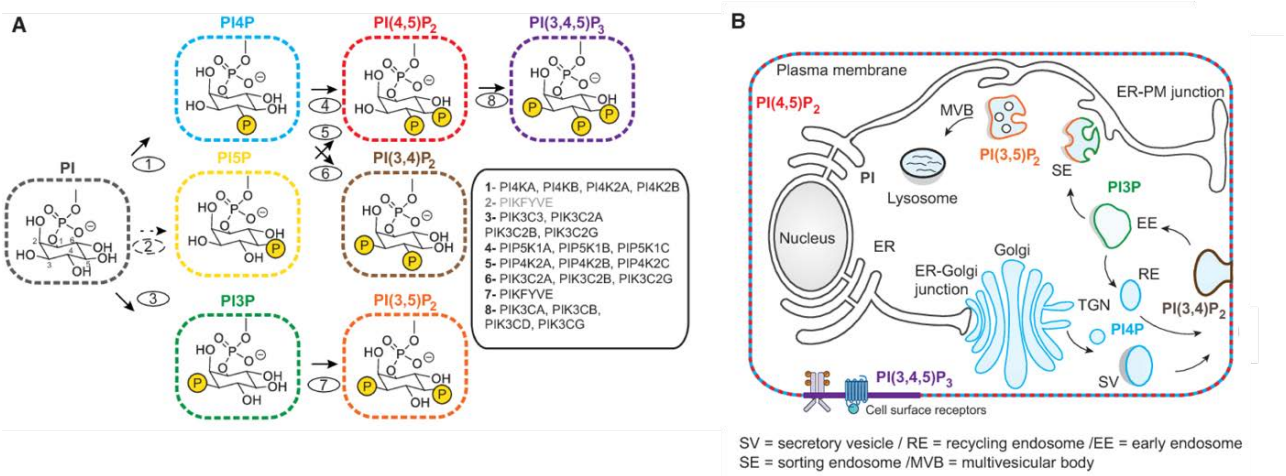

Figure 1. Phosphoinositide species and their subcellular localization. (A) A schematic depicting the generation of each species of phosphoinositide; numbers indicate the gene encoding the phosphoinositide kinase that generated that species. (B) The cellular localization of different phosphoinositides. Adapted from Burke, 2018.

Phosphatidylinositol 4-phosphate (PI4P) is one of the most abundant species of phosphoinositides in mammalian cells and can be found predominantly at the plasma membrane (PM) (Mesmin et al., 2017). PI4P is generated via phosphorylation of the 4′ position on the

inositol headgroup of PI and is exchanged for PS via lipid transporters at the endoplasmic reticulum (ER) at ER-PM contact sites (Chung et al., 2015). This exchange is essential for enrichment of ER-synthesized lipids on the PM as it helps maintain the membrane heterogeneity that is essential for proper cell trafficking. Therefore, PI4P is an essential signaling molecule for maintaining PM lipid asymmetry (Chung et al., 2015).

The Structure and Activation of PI4KA

Phosphorylation of PI to generate PI4P is catalyzed by the enzyme phosphatidylinositol 4-kinase (PI4K), a peripheral membrane protein. There are four types of PI4Ks found in humans, which are categorized as either type II or type III (Boura & Nencka, 2015). Type III PI4Ks have two isoforms, phosphatidyl 4-kinase IIIα (PI4KA) and phosphatidylinositol 4-kinase IIIβ (PI4KB). PI4KA is responsible for generating the pool of PI4P at the PM, ensuring successful exchange of heterogeneous lipids, as well as proper recruitment of transport vesicles and peripheral membrane proteins (G. R. V. Hammond et al., 2012). Furthermore, PI4P generated at the PM can be converted into the downstream phosphoinositides phosphatidylinositol 4,5 bisphosphate (PIP_2) and phosphatidylinositol 3,4,5 trisphosphate (PIP_3), which play important roles in signaling pathways involving phospholipase C and Akt kinase, respectively (Dornan et al., 2018a; Hemmings & Restuccia, 2012).

The structure of PI4KA includes four key regions: the alpha solenoid, dimerization domain, helical domain, and kinase domain, as shown in figure 2. The alpha solenoid is responsible for several protein-protein interactions to help confer structural stability, while the helical and kinase domains give PI4KA its catalytic activity. Additionally, PI4KA associates with two accessory proteins: tetratricopeptide repeat domain 7 (TTC7) and FAM126, which each have two isoforms: TTC7A/B and FAM126A/B, and come together with PI4KA to form a trimer

(Baskin et al., 2016; Lees et al., 2017). TTC7 has three contact points with PI4KA, the first being the C-terminal helix of TTC7, which associates with the N-terminal tip of the alpha solenoid of PI4KA. TTC7 also interacts with the dimerization domain of PI4KA, as well as the cradle surrounding the catalytic domain (Lees et al., 2017). These interactions are essential for correct functionality and localization of PI4KA (Nakatsu et al., 2012). FAM126 is peripheral to PI4KA and acts as a central scaffold to TTC7, and does not interact with PI4KA directly (Baskin et al., 2016). Through the dimerization domain of PI4KA, two trimers come together to form a dimer of heterotrimers, resulting in a complex of about 700 kDa (Dornan et al., 2018; Lees et al., 2017).

A testament to their importance, PI4KA and TTC7 have been conserved across evolutionary history, and have been extensively studied in yeast (Baird et al., 2008). Notably, FAM126 is not conserved across all eukaryotic evolution as it is not observed in some organisms, such as fungi (Baskin et al., 2016). Stt4, the yeast homolog of PI4KA, has been shown to interact directly with Ypp1, the yeast homolog of TTC7, and stabilize PI4KA so it can produce pools of PI4P at the PM. An integral membrane protein, EFR3, has also been shown to interact with Ypp1. Yeast EFR3 has been shown to localize to the PM, even in the absence of Stt4 and Ypp1 (Baird et al., 2008). When Ypp1 is absent in yeast, Stt4 is mislocalized to the cytoplasm and degraded, failing to produce pools of PI4P at the PM. A similar observation is seen when yeast EFR3 is absent in cells: Stt4 is again mislocalized. As such, it has been proposed that EFR3 is anchored to the PM, and recruits the Stt4/Ypp1 complex to produce PI4P (Baird et al., 2008).

Given this information, the putative mechanism of recruitment for the mammalian PI4KA complex to the PM involves the mammalian homolog of EFR3. In mammals, EFR3 has two

isoforms, EFR3A/B. The C-terminus of EFR3A interacts with TTC7B and FAM126A within the PI4KA regulatory complex, while the palmitoylated N-terminus is embedded in the PM (Baskin et al., 2016; Bojjireddy et al., 2015). Taken together, these findings indicate that EFR3A is an activator of PI4KA via its recruitment to the PM (Wu et al., 2014).

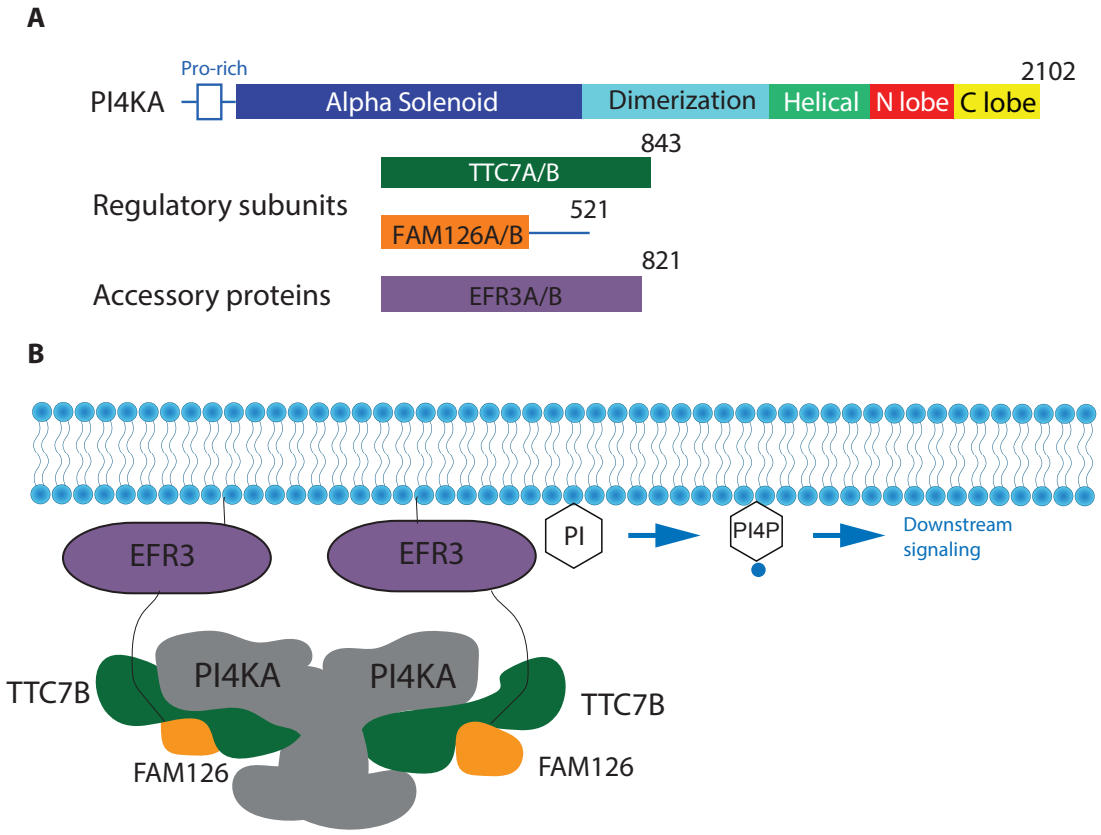

Figure 2. The PI4KA regulatory complex and its accessory proteins. (A) The domain architecture of the PI4KA, along with its regulatory subunits and accessory proteins. Adapted from Burke & McPhail (2022). (B) The putative mechanism for the recruitment of the PI4KA complex to the PM by EFR3.

PI4KA in Disease

Proper function of PI4KA is essential in eukaryotes. Published work by Bojjireddy et al., (2014) has shown that inhibition of PI4KA in vitro decreased the levels of PI4P in cells, and large doses of PI4KA inhibitors was lethal in mouse models. Additionally, the

authors also tested the importance of PI4KA by knocking out the PI4KA gene by targeting exon 48, resulting in a catalytically inactive protein. Lethal epithelial cell necrosis was observed in knockout mouse models. The authors postulated that downstream effectors deplete existing pools of PI4P, and without PI4KA, downstream signaling molecules such as PIP_2 cannot be replenished. G-protein coupled receptors involved in maintaining vascular tone rely on these pools of PIP_2 and fail in their absence, resulting in the death of the mouse models (Bojjireddy et al., 2014).

PI4KA has been linked to several diseases, including cancer and viral infection. The KRAS gene, along with related genes HRAS and NRAS, are mutated in a fifth of human cancers (Prior et al., 2020). These three genes encode four ubiquitously expressed proteins, the latter of which can be spliced into KRAS4A and KRAS4B. All are part of the Ras protein family. These proteins act as molecular switches, and control signaling pathways that are involved in cell proliferation and survival (Mo et al., 2018). Interestingly, targeting oncogenic KRAS has been shown to have therapeutic potential in human trials, and as such has been studied further by Adhikari et al., (2021). Since these Ras species are signaling proteins found predominantly at the PM, they are under strict regulation. It has been shown that a PI4P concentration gradient maintains KRAS localization and nanoclustering at the PM, which is established by the exchange of PS at ER-PM contact sites. Furthermore, the authors showed that oncogenic KRAS associates with EFR3A, and that loss of EFR3A or PI4KA reduces the levels of PI4P at the PM. Loss of EFR3A also reduced KRAS localization to the PM. The authors propose a positive feedback mechanism, whereby oncogenic KRAS binds EFR3A which recruits PI4KA and stimulates PI4P production, promoting KRAS localization to the PM, and allowing for oncogenic signaling (Adhikari et al., 2021).

PI4KA has also been linked to viral infection. Successful Hepatitis C Virus (HCV) infection requires PI4P production at replication organelles to enrich sterol and sphingolipid species (McPhail & Burke, 2022). HCV will recruit and activate PI4KA, which binds to the viral NS5A protein. Importantly, silencing of PI4KA significantly reduced HCV replication and release, offering a potential target for future therapeutics (Lim & Hwang, 2011).

Biolayer Interferometry

A method that can be used to study protein-protein interactions is biolayer interferometry (BLI). BLI is a tool that allows for the study of protein complex formation in real time, to determine the kinetic parameters of the interaction. Protein is bound to the sensor tips via affinity tags often used for protein purification, such as 6xHIS or streptavidin. After sample loading, the sensor tip with the ligand protein is allowed to equilibrate in buffer before being dipped into the sample protein (the analyte). The kinetics of the interaction can be indirectly determined by measuring the wavelength shift of white light that is reflected at the optical sensor, located above the sensor tips. The change in wavelength is calculated from two measurements: first, the wavelength reflected from the ligand protein with no analyte, followed by the wavelength reflected from the ligand protein with the sample protein bound to it. The difference in wavelength ($\Delta\lambda$) is detected by the instrument, which takes multiple readings over time. The dissociation constant (KD) can be determined from this information. This assay is advantageous because it requires less protein than other methods that characterize protein interactions, such as surface plasmon resonance or isothermal titration calorimetry. This makes BLI an ideal method to use, especially when assessing proteins that are difficult to purify and express. A schematic of BLI is outlined in figure 3 (Orthwein et al., 2021). Each step of the BLI assay is essential for

accurate interpretation of results. The shift in wavelength measured before and after analyte interaction is compared and the KD of the interaction is calculated by forcing 1:1, site specific binding between the ligand protein and the analyte.

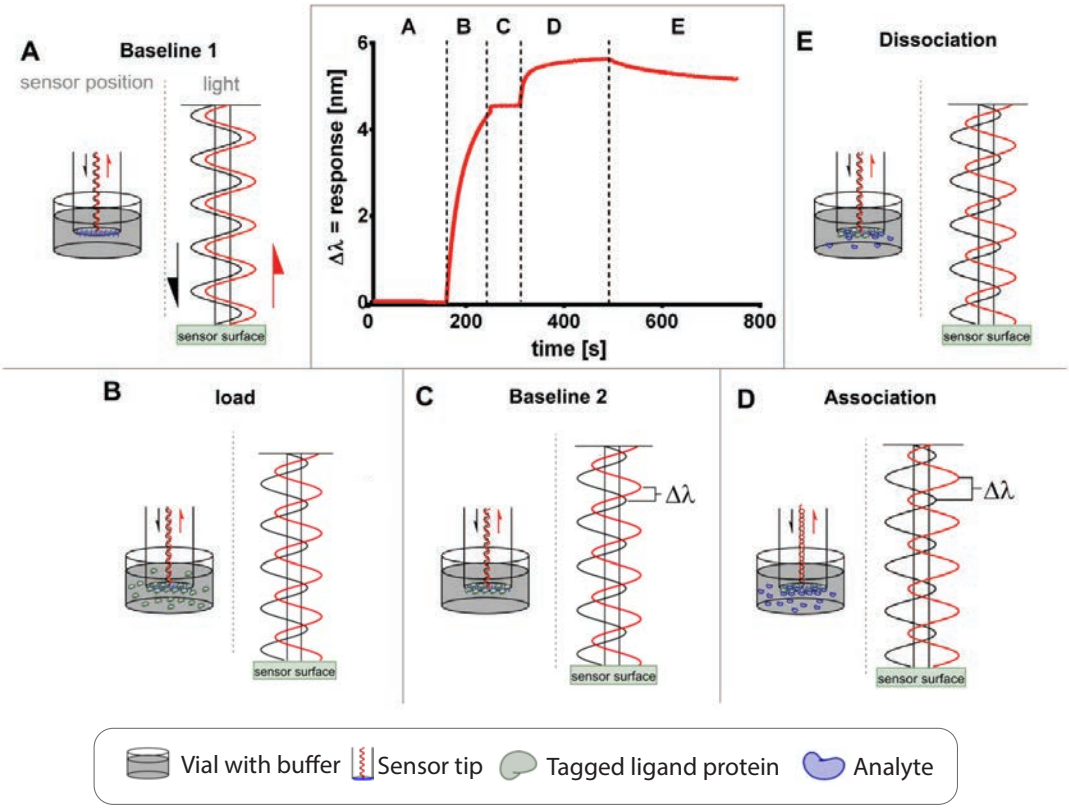

Figure 3. A representative schematic of a biolayer interferometry assay. The shift in wavelength is represented by Δλ. (A) Baseline 1. The sensor alone is allowed to equilibrate in BLI buffer. (B) Load. The tagged ligand proteins, suspended in buffer, are loaded onto the probe. (C). Baseline 2. The loaded sensor is placed back in BLI buffer. (D) Association. The probe, loaded with tagged protein, is dipped into BLI buffer containing analyte protein. (E) Dissociation. The probe is then placed back into BLI buffer. Adapted from Orthwein et al., (2021).

Previous Work

Continuation with the TTC7B/FAM126A dimer.

Published data from Baird et al., (2008) and Nakatsu et al., (2012) had established that the Stt4, the yeast homolog of PI4KA, is recruited to the PM through the interaction with Ypp1 (yeast homolog of TTC7B). However, EFR3 alone was not enough to recruit Stt4 to the PM, resulting in mislocalization of Stt4 in the cytoplasm. Using this information, it was concluded that the C-terminal tail of EFR3 only interacts with the accessory proteins of the PI4KA regulatory complex, and not the kinase itself (Wu et al., 2014). Before the work of this thesis was completed, previous lab members used this information to guide a series of gel filtration experiments using the human homologs of the complex. They demonstrated that the interaction between EFR3A and the PI4KA regulatory complex could be studied using only the TTC7B/FAM126A dimer, as illustrated in figure 4. A new construct of the dimer, which included full-length TTC7B and truncated FAM126A (2-308) was generated, expressed, and purified. This construct will further be referred to as TTC7B/FAM126A. A new construct of the EFR3A C-terminal tail was also produced and contained residues 721-791. This construct will further be referred to as EFR3A. TTC7B/FAM126A and EFR3A were run separately on a Superdex 200 10/300 increase gel filtration column to confirm the expected elution volume. Following this, the TTC7B/FAM126A dimer and EFR3A were loaded onto the column and gel filtered simultaneously; EFR3A was found to co-elute with TTC7B/FAM126A as evidenced by a shift in elution volume (figure 4). This experiment confirmed that EFR3A does interact with the

TTC7B/FAM126A dimer in the absence of PI4KA.

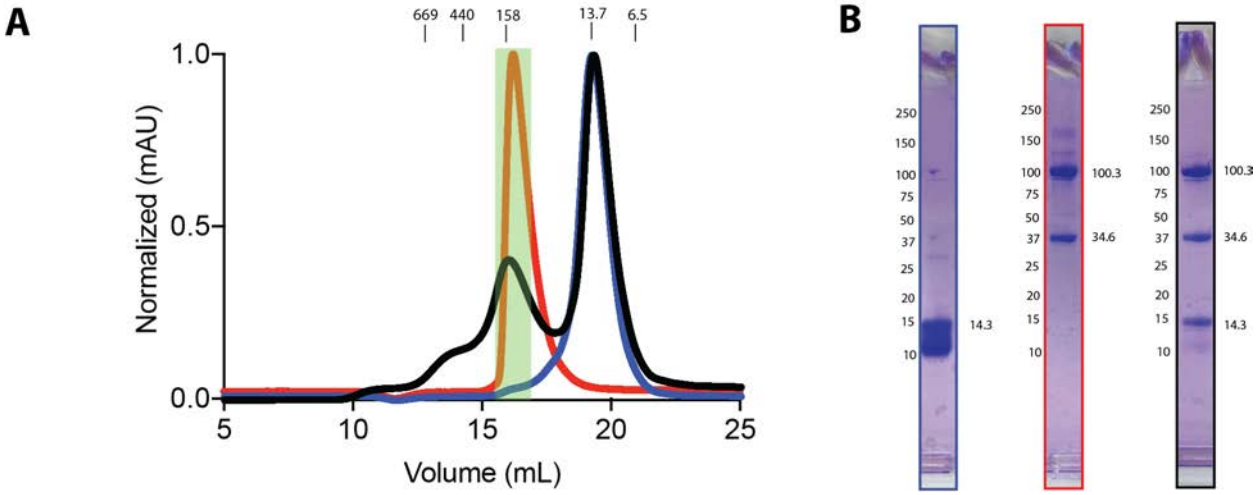

Figure 4. Gel filtration of TTC7B/FAM126A (2-308) and EFR3A (721-791). (A) Gel filtration traces of apo EFR3A (blue), apo TTC7B/FAM126A (red), and the combined TTC7B/FAM126A/EFR3A trace (black). (B) SDS-PAGE fractions taken at the peaks of the apo EFR3A (blue) and apo TTC7B/FAM126A (red) gel filtration traces. The green box indicates where the combined TTC7B/FAM126A/EFR3A fraction (black) was taken.

Calculation of the dissociation constant (KD).

A dose-response BLI assay was done to determine the K_D of TTC7B/FAM126A bound to EFR3A, as shown in figure 5. His-tagged EFR3A was bound to the probe, and purified TTC7B/FAM126A was allowed to associate with the EFR3A on the probe. 1:1, site specific binding between the ligand protein and the analyte was used to calculate the K_D, which was determined to be about 300 nM.

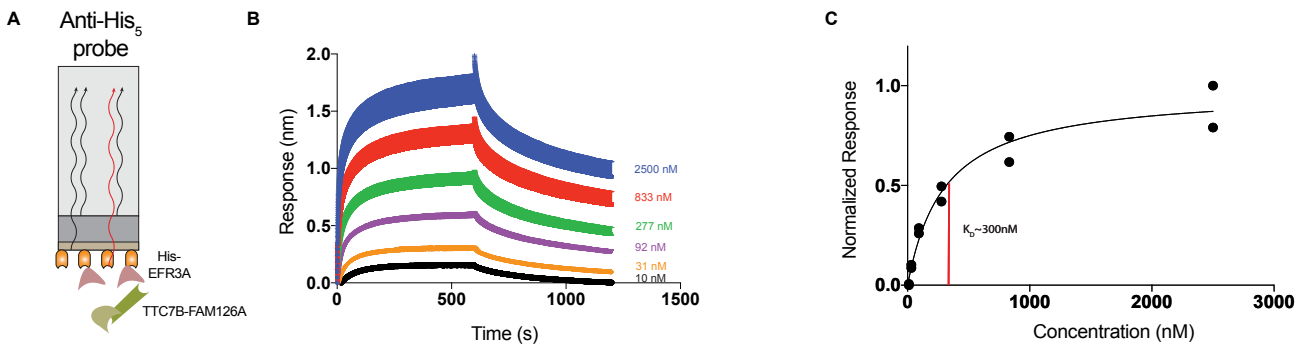

Figure 5. Determination of the dissociation constant (KD). (A) Association and dissociation curves of dose-response assay measured using BLI. Different colours indicate the different concentrations of TTC7B-FAM126A dimer used. (B) Responses fit to a normalized curve, showing saturation of EFR3A by TTC7B-FAM126A, which was used to determine the KD.

Structural prediction using AlphaFold.

AlphaFold is an artificial intelligence software that predicts protein structure based on its amino acid sequence. Developed by DeepMind, it uses the information from multiple sequence alignments, co-evolutionary information, and existing structural information to generate an accurate prediction (Jumper et al., 2021; Varadi et al., 2022). Lab members used AlphaFold to predict the binding interface between TTC7B/FAM126A and the C-terminal tail of EFR3A, as seen in figure 6.

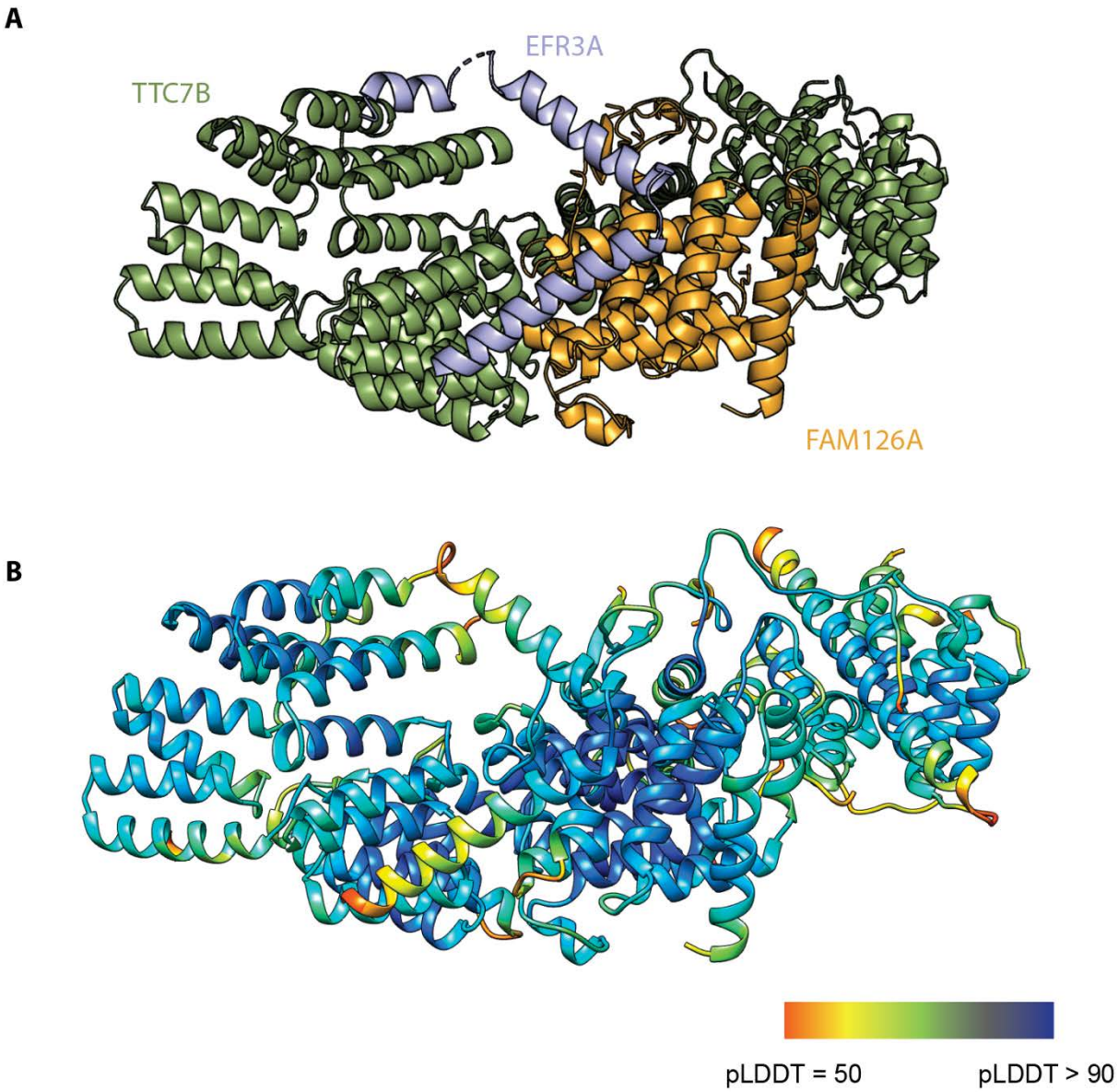

Figure 6. AlphaFold generated consistent models. (A) Predicted structure colored according to protein chain. (B) Predicted structure with pLDDT confidence mapped according to the legend.

Research Objective

The goal of this study was to investigate the structural basis for interaction and recruitment of the PI4KA regulatory complex and the membrane protein EFR3A. BLI was used to establish the KD of the interaction between EFR3A and TTC7B/FAM126A; AlphaFold was

used to predict the binding interface. Using the structural prediction generated using AlphaFold and multiple sequence alignments, residues predicted to be important for the interaction were mutated; interaction with the wild type binding partner was assessed using BLI. Future work will be directed towards further refinement and development of additional mutations to validate the AlphaFold model.

Methods

Sequence Alignment

Sequences were aligned using Clustal Omega Multiple Sequence Alignment, which was then analyzed by ESPript 3.0 to visualize conserved regions. The accession numbers are as follows; EFR3A: Q14156 (human), Q8BG67 (mouse), Q641A2 (frog), QUIGJ0 (fruit fly), Q09263 (flatworm), Q03653 (yeast), TTC7B: Q86TV6 (human), E9Q6P5 (mouse), A0A8J1LPX2 (frog), A0A0B4K7H0 (fruit fly), H2KYB6 (flatworm), P46951 (yeast), FAM126A: Q9BYI1 (human), Q6P9N1 (mouse), Q5HZS6 (frog), Q6P121 (zebrafish).

Plasmids and Primers

Plasmids encoding for the C-terminus of wild ype EFR3A (residues 721-791) and the TTC7B/FAM126A dimer (full-length TTC7B, FAM126A residues 2-308) were made by previous lab members. Both constructs included an N-terminal 2x strep tag and 10x His tag, cleavable by TEV protease for purification purposes, along with ampicillin resistance to ensure proper plasmid uptake by *Escherichia coli* cells. Primers were designed to incorporate a single residue mutation into the wild type plasmids, as listed in Table 1. Mutagenesis was performed via PCR, the resulting plasmids were transformed into *E.coli* XL10 cells using heat shock, and then selected for ampicillin resistance. Isolated colonies were picked and left to grow in 5 mL liquid culture with ampicillin for 16 hours. Plasmids were isolated using a Monarch miniprep kit from New England Biolabs; successful mutagenesis of the wild type plasmid was confirmed by

Plasmidsaurus. The plasmids were then transformed into *E. coli* C41 cells and selected for ampicillin resistance.

Table 1. Primers used for protein mutagenesis. Primers used in mutagenesis reactions to generate mutant residues along the binding interface between EFR3A (721-791) and the TTC7B/FAM126A (2-308) dimer. The plasmid ID, primers, and associated mutations are listed along with the protein mutated.

Plasmid	Protein	Primers	Mutation
SS88	EFR3A	F: 5'- CCTTTGAAGCACTGGAAAAGGCCATTGATACCAGCGGT -3' R: 5'- CAGTGCTTCAAAGGTAATTTCTTCGGTG -3'	K732E
SS89	EFR3A	F: 5'- CCGAAGAAATTACCGCTGAAGCACTGAAAAAGGCCATTGATACC-3' R: 5'- GGTAATTTCTTCGGTGTTGCTACCTGC -3'	F728A
SS90	EFR3A	F: 5'- CTGGTCATCGAAAAAGCTCAGAAAGCACCGTTTGAAGAAATTGC -3' R: 5'-TTTTTCGATGACCAGGCGACG -3'	F755A
SS91	EFR3A	F: 5'- AGAAAGCACCGGCTGAAGAAATTGCAGCACAGTGTGAAAGC -3' R: 5'- CGGTGCTTTCTGAAATTTTTCGATGACC -3'	F760A
SS99	EFR3A	F: 5'- ACCTTTGAAGCAGCGAAAAAGGCCATTGATACCAGCGG -3' R: 5'- TGCTTCAAAGGTAATTTCTTCGGTGTTG -3'	L731A
SS102	EFR3A	F: 5'- CACCGTTTGAAGAAGCTGCAGCACAGTGTGAAAGCAAAGC -3' R: 5'- TTCTTCAAACGGTGCTTTCTGAAATTTTTCG -3'	I763A
SS113	TTC7B	F: 5'- TGTAAGCACATGGCGCAGATATGGAAATCCTGCTACAACCTCA -3' R: 5'- CATGTGCTTACAAGTCAGCAGTGC -3'	L610A
SS115	TTC7B	F: 5'- TCTGGGGTATGTCGAGCAAGCTCTTCAGCTTCAAGGTGACG -3' R' 5'- GACATACCCCAGAGCCTCTGG -3'	R539E
SS103	TTC7B	F: 5'- GGCACAGATCGCCCTCCATGCAGCTGAAGTCTATATCGG -3' R: 5'- GATCTGTGCCAGCGTCATCC -3'	W699A
SS104	FAM126A	F: 5' - CTAGAACCTGTCTGTGAGCAGCTCTTTGAATTCTATCGCAGTGG -3' R: 5' - ACAGACAGGTTCTAGCAACTCACTTTG -3'	H58E
SS105	FAM126A	F: 5'- GCATTGAAGCTCTTCTTTTTGGGGTTTACAATTTGGAAATAGTTGACAAACAG -3' R: 5'- AAGAAGAGCTTCAATGCATCCACTG -3'	L106F
SS106	FAM126A	F: 5'- GGCACAGATCGCCCTCCATGCAGCTGAAGTCTATATCGG -3' R: 5'- GATCTGTGCCAGCGTCATCC -3'	F61A

Protein Expression

The EFR3A and TTC7B/FAM126A constructs were expressed in *E. coli* C41 cells. Plasmids designed to express EFR3A (721-791) were induced with 0.5 mM IPTG (isopropyl β-D-1- thiogalactopyranoside) and incubated for 3 h at 37°C. Plasmids designed to express the TTC7B/FAM126A (2-308) dimer were induced with 0.1 mM IPTG and incubated at 21°C for 20 hours. Cells were then centrifuged at 3900 rpm; pellets were stored at -80°C for future use.

Protein Purification

To purify TTC7B/FAM126A, wild type and mutants, *E. coli* cell pellets were sonicated for 5 minutes (10 seconds on and 10 seconds off) in lysis buffer (20 mM imidazole pH 8, 100 mM NaCl, 5% (v/v) glycerol, 2 mM β-mercaptoethanol (bME), and protease inhibitors (Millipore Protease Inhibitor Cocktail Set III, EDTA (ethylenediaminetetraacetic acid)-free)). Triton X-100 was added to the lysate to 0.1% (v/v) and the solution was centrifuged for 45 minutes at 14,000 RPM at 4°C for 45 minutes. A 5 mL HisTrap™ column (GE Healthcare) was equilibrated with NiNTA A buffer (20 mM imidazole pH 8, 100 mM NaCl, 5% (v/v) glycerol, 2 mM bME). The supernatant was poured off the pellet, filtered, and loaded onto the column. The column was then washed with 20 mL NiNTA A buffer, 20 mL 6% NiNTA B buffer (450 mM imidazole pH 8, 100 mM NaCl, 5% (v/v) glycerol, 2 mM bME)). The protein was then eluted off the column using 15 mL 100% NiNTA B buffer. A 5 mL StrepTrap™ column was equilibrated with 15 mL water and 15 mL GFB buffer (20 mM imidazole pH 7, 150 mM NaCl, 0.5 mM tris(2-carboxyethyl)phosphine (TCEP), 5% glycerol). The 15 mL eluate from the nickel purification was loaded on to the column and washed with 15 mL GFB. 5 mL GFB plus Lip-TEV (tobacco etch virus) was loaded onto the column, which was left on ice and placed in a 4°C cabinet to cleave overnight. The following day, the protein was eluted from the column using 15

mL GFB. The eluate was then placed in an Amicon 30K concentrator before being loaded onto a Superdex 200 10/300 GL column for size exclusion chromatography (SEC), which was equilibrated with GFB. The entire sample of concentrated protein was loaded and run on the AKTA, fractions were collected and concentrated in an Amicon 30K concentrator. The protein was then flash frozen in liquid nitrogen and stored at -80°C.

To purify EFR3A (wild type and mutants), *E. coli* cell pellets were sonicated for 5 total minutes (10 seconds on and 10 seconds off) in lysis buffer (20 mM Tris pH 8, 20 mM imidazole pH 8, 100 mM NaCl, 5% (v/v) glycerol, 2 mM bME, and protease inhibitors (Millipore Protease Inhibitor Cocktail Set III, EDTA-free). Triton X-100 was added to the lysate to 0.1% (v/v) and the solution was centrifuged for 45 minutes at 14,000 RPM at 4°C for 45 minutes. A 5 mL HisTrap™ column (GE Healthcare) was equilibrated with NiNTA A buffer (20 mM Tris pH 8, 20 mM imidazole pH 8, 100 mM NaCl, 5% (v/v) glycerol, 2 mM bME). The supernatant was poured off the pellet, filtered, and loaded onto the column. The column was washed with 20 mL high salt buffer (20 mM Tris pH 8, 1 M NaCl, 10 mM imidazole, 5% glycerol, 2 mM bME), 15 mL NiNTA A, 15 mL 6% NiNTA B (20 mM Tris pH 8, 100 mM NaCl, 250 mM imidazole pH 8, 2 mM bME). The protein was eluted from the column using 17 mL 100% NiNTA B. A 5 mL StrepTrap™ column was equilibrated with 15 mL water followed by 15 mL GFB (20 mM HEPES (4-(2-hydroxyethyl)-1-piperazineethanesulfonic acid) pH 7.5, 150 mM NaCl, 0.5 mM TCEP, 5% glycerol). The nickel eluate was loaded onto the column, which was washed with 10 mL GFB plus 0.5 M NaCl, then with 5 mL ATP mixture (2 mM ATP, 10 mM $MgCl_2$, 150 mM KCl, 20 mM HEPES pH 7.5, 150 mM NaCl, 0.5 mM TCEP, 5% glycerol), then with 10 mL GFB. The protein was eluted using GFB plus 2.5 mM desthiobiotin and concentrated in an Amicon 10 K concentrator. A Superdex 75 10/300 increase gel filtration column was

equilibrated using GFB, the entire protein sample was loaded and run on an AKTA size exclusion liquid chromatography system. Fractions were collected and concentrated further using an Amicon 10K concentrator; the protein was then snap frozen in liquid nitrogen and stored at -80°C.

Biolayer Interferometry

A Fortebio (Sartorius) K2 Octet system was used for all biolayer interferometry assays. Anti-penta-His biosensors were loaded with either wild-type or mutant EFR3A. Prior to starting the assays, the biosensors were incubated in BLI buffer (20 mM HEPES pH 7.5, 150 mM NaCl, 0.01% BSA, 0.002% TWEEN-20) for 10 minutes. The steps of each assay were identical, and proceeded as follows: regeneration, neutralization custom, loading, baseline, association, and dissociation. Glycine pH 1.5 was used for regeneration, and BLI buffer was used for neutralization. The same biosensor was used for technical replicates, which was regenerated by dipping the biosensor back and forth between glycine pH 1.5 and BLI buffer six times (five seconds each) The steps outlined above were then repeated either once or twice for duplicate or triplicate experiments. Within each replicate, the custom, baseline, and dissociation steps all used the same well of BLI buffer. EFR3A was diluted to 200 nM and added to the loading wells; TTC7B/FAM126A was diluted to 500 nM and added to the association wells. Each experiment was done at 25°C with shaking at 1000 rpm.

Results

Sequence Alignments

Sequence alignment was used to supplement the AlphaFold model by providing information on the conservation of residues for each binding partner, as shown in figure 7. Conservation through evolutionary history indicates that the residue is important for maintaining a functional interaction at the binding interface between TTC7B/FAM126A.

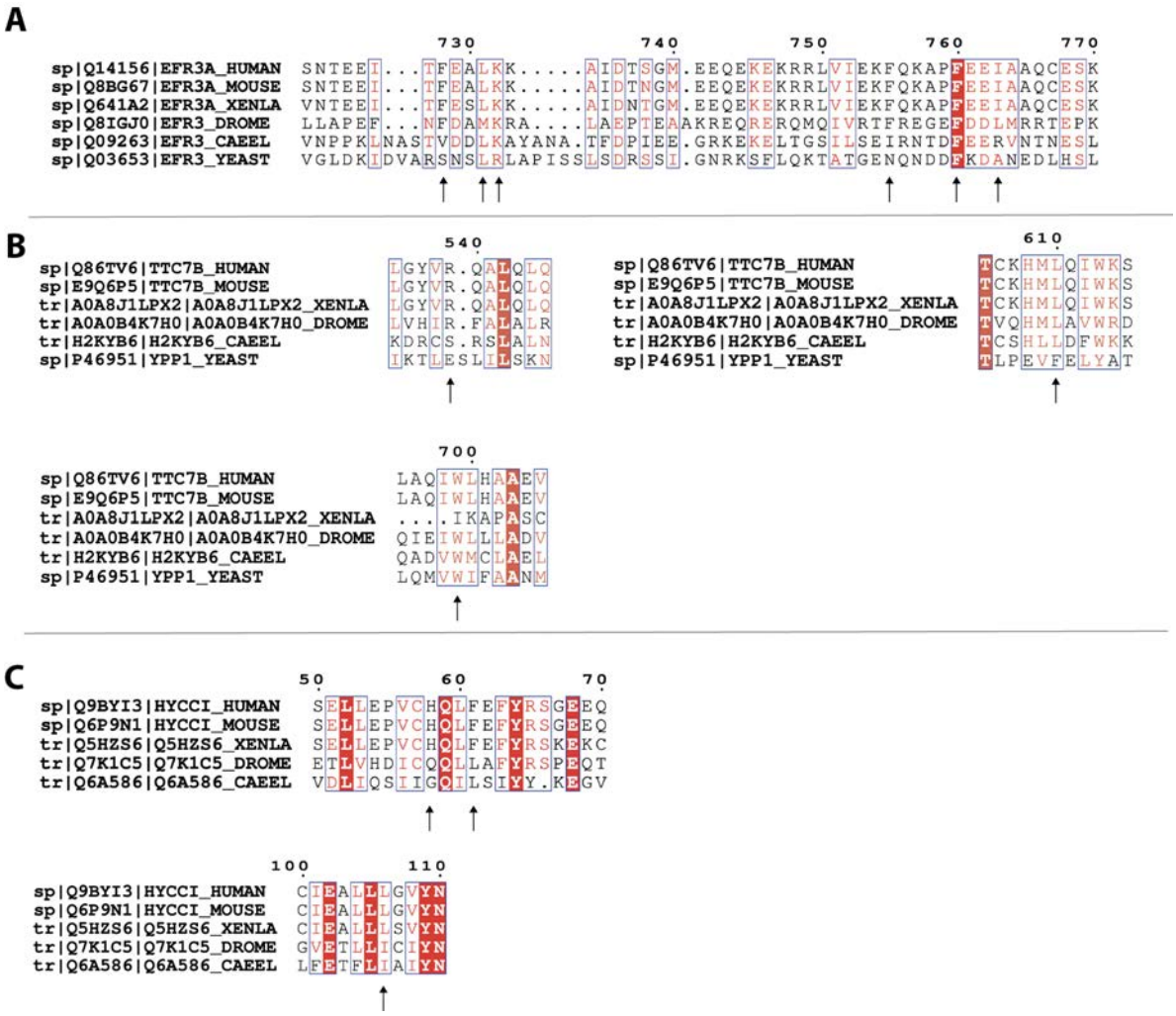

Figure 7. Sequence alignments of EFR3A, TTC7B, and FAM126A. Sequences were aligned using the Clustal omega tool; arrows indicate mutated residues. (A) EFR3A residues 720-770, with mutants generated at F728, L731, K732, F755, F760, and I763. (B) TTC7B residues 535-540, 605-615, and 695-705, with mutants generated at R539, L610, and W699. (C) FAM126A residues 50-70 and 100-110, with mutants generated at H58, F61, and L106.

Protein Purification

Purification of EFR3A C-terminus.

Following successful expression of EFR3A constructs in *E. coli*, purification was carried out using HisTrap and StrepTrap affinity columns. The protein was eluted from the StrepTrap affinity column using 2.5 mM desthiobiotin, which outcompetes the protein for streptavidin binding sites, effectively eluting the protein. Subsequent gel filtration and SDS-PAGE gel electrophoresis showed an abundance of degraded EFR3A. Upon preparation, small fractions of the largest peak were taken during gel filtration, as indicated by the coloured boxes in figure 8. After running these fractions on an SDS-PAGE gel, we decided that the optimal C-terminal construct of EFR3A eluted from the shoulder of the main peak in the gel filtration trace. This step was necessary to optimize EFR3A C-terminal stability for use in subsequent experiments. Figure A5, listed in the appendix, shows the variability between wild type preps and day-to-day variability.

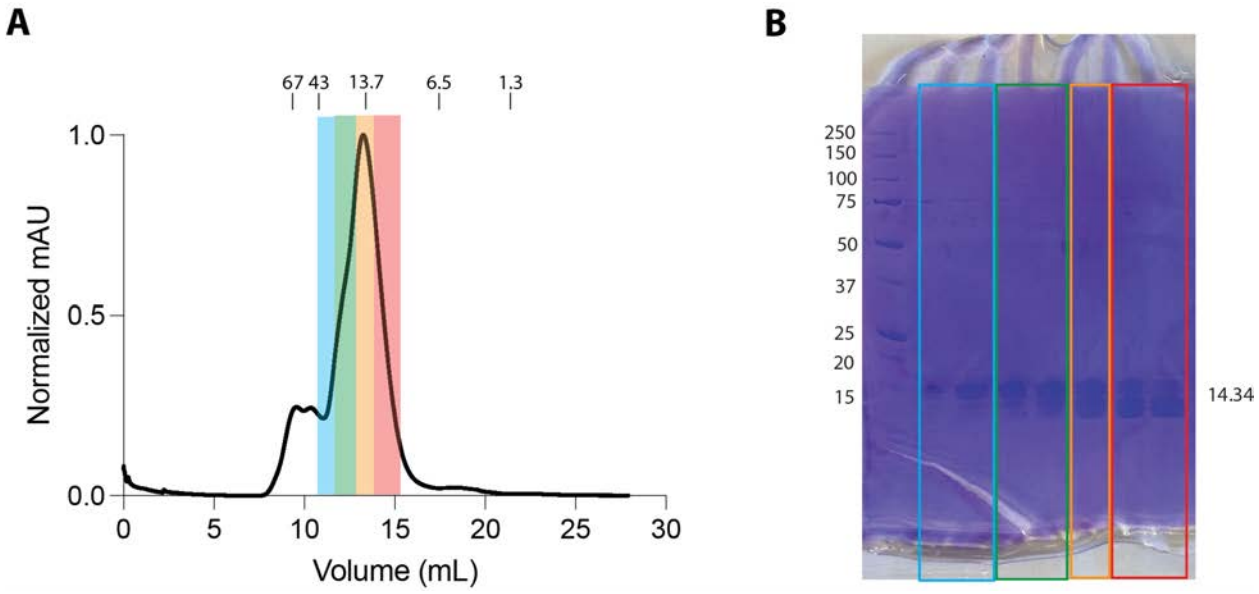

Figure 8. Purification of EFR3A (721-791) C-terminus. (A) Size exclusion chromatography trace of wild-type EFR3A prep 1, run on a Superdex 75 Increase 10/300 GL size exclusion column. Coloured boxes indicate the fractions taken upon purification, samples of which were run on the SDS-PAGE gel shown in (B).

Subsequent preps of wild type EFR3A were expressed and purified in a similar fashion, as seen in figure 9.

Purification of the TTC7B/FAM126A dimer.

Following successful recombination of TTC7B/FAM126A constructs in *E. coli,* purification was carried out using HisTrap and StrepTrap affinity columns. TTC7B/FAM126A dimer was cleaved from the StrepTrap affinity column using Lip-TEV protease, to remove the His and Strep tags. Gel filtration and SDS-PAGE gel electrophoresis revealed that the wild type protein was relatively stable during preparation and purification. Gel filtration showed that the main peak of TTC7B/FAM126A was consistent with an elution profile of a dimer; fractions of the main peak were taken as seen in figure 10, and used in subsequent experiments.

Size exclusion chromatography traces and uncropped SDS-PAGE gels of all mutant proteins are listed in the Appendix.

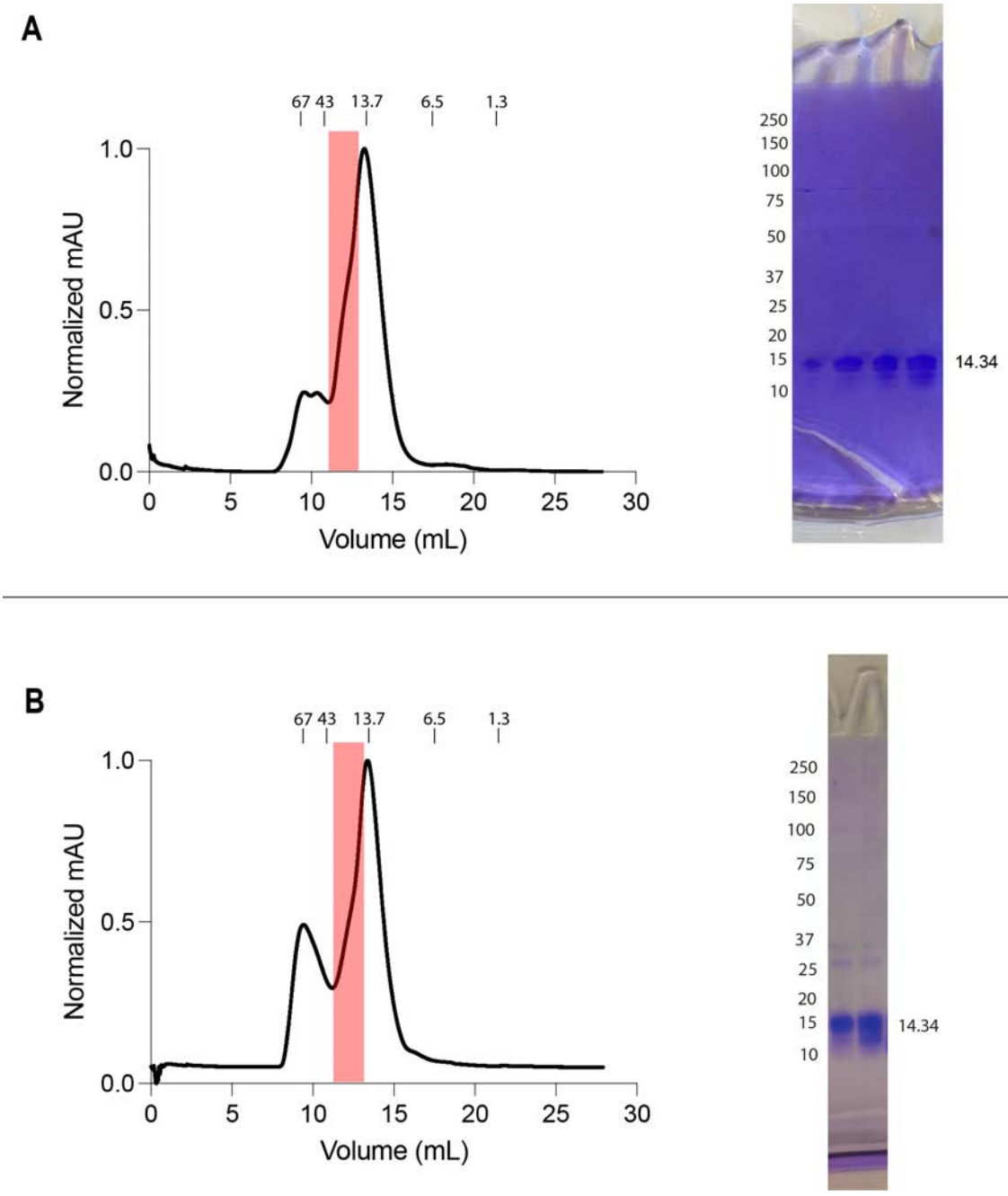

Figure 9. Purification of EFR3A (721-791) wild type constructs. Red box indicates the fractions taken upon purification; samples of each fraction were run on the adjacent SDS-PAGE gel. (A) Size exclusion chromatography trace of wild-type EFR3A prep 1, run on a Superdex 75 Increase 10/300 GL size exclusion column. (B) Purification of EFR3A prep 2, run on a Superdex 75 Increase 10/300 GL size exclusion column.

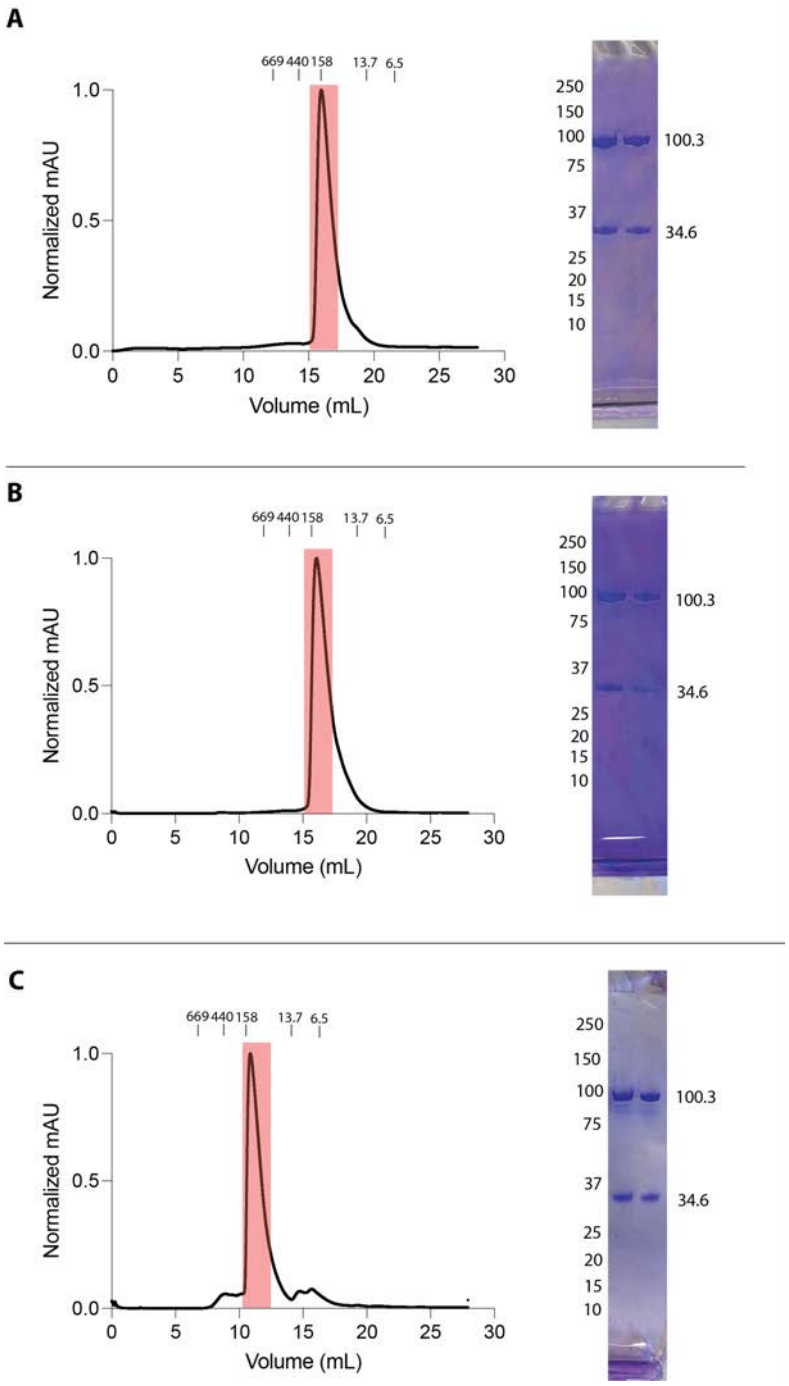

Figure 10. Purification of TTC7B/FAM126A (full-length TTC7B, FAM126A 2-308). The red boxed indicate the fractions taken upon purification; samples of each fraction were run on the adjacent SDS-PAGE gel. (A) Size exclusion chromatography trace of wild-type TTC7B/FAM126A prep 1, run on a Superose 6 Increase 10/300 GL size exclusion column. (B) Purification of TTC7B/FAM126A prep 2, run on a Superose 6 Increase 10/300 GL size exclusion column. (C) Purification of TTC7B/FAM126A prep 3, run on a Superdex 200 10/300 GL size exclusion column.

Mutations of Putative Interface Residues Disrupt Binding

Using the AlphaFold model of the EFR3A C-terminus in complex with the TTC7B/FAM126A dimer as a guide, mutations in putative contact sites were generated and tested using BLI. A two-tailed T-test with Welch's correction was used to test the null of no difference between the wild type and the given mutant, with alpha set to 0.05.

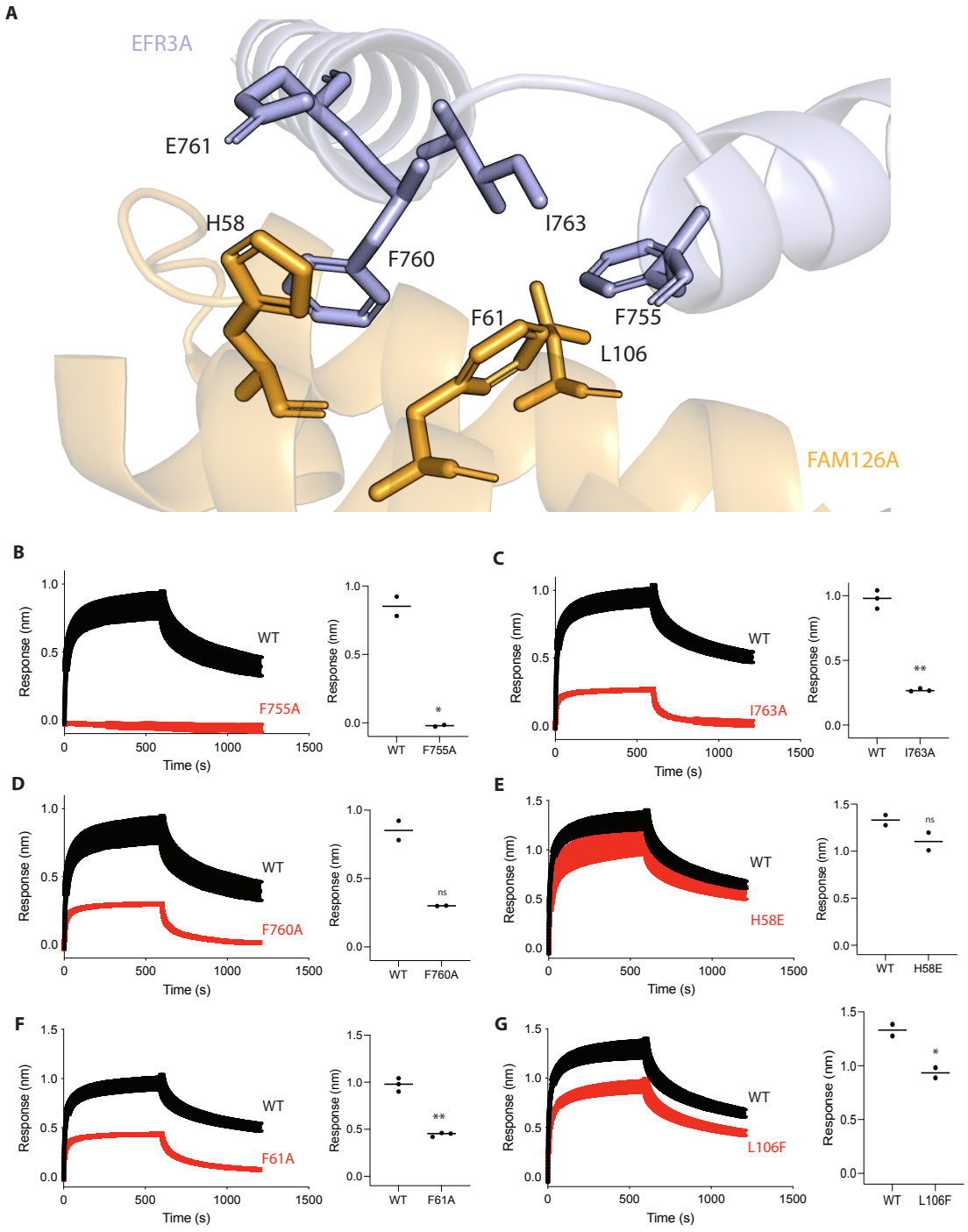

Figure 11. Mutations at the predicted EFR3A (721-791)/FAM126A (2-308) interface disrupt binding. (A) A subsection of the predicted binding interface between EFR3A and FAM126A (2-308), generated using AlphaFold. (B-G) BLI measurements taken during association and dissociation of wild-type protein and the respective mutant. 200 nM EFR3A was

loaded onto the optical fiber tip. TTC7B/FAM126A was tested at 500 nM. Mutants were statistically compared to wild-type binding using a two-tailed T-test with Welch's correction. ns = no significance, * = $P < 0.05$, ** = $P < 0.01$.

The mutations generated along the predicted binding interface likely form salt bridging interactions or associate via hydrophobic interactions. F755, F760, and I763 on EFR3A are likely interacting with other hydrophobic residues on FAM126A, such as F61 and L106, as shown in figure 11. F755A, F760A, and I763A were all generated to disrupt this binding niche. F755A had a significant effect on binding ($P = 0.0496$), with a complete reduction of the response to 0. I763A also significantly disrupted binding ($P = 0.0052$); with an observed 4-fold reduction in response. Although F760A had a marked effect on binding, with an observable 3.2-fold decrease in association, we failed to reject the null of no difference ($P = 0.0805$).

Based on the AlphaFold model, the corresponding mutations in FAM126A were also generated, to see if they disrupted binding. L106F showed a significant effect on binding ($P = 0.0322$), as did F61A ($P = 0.0032$), indicating that the hydrophobic residues responsible for the interaction between EFR3A and FAM126A had been successfully disrupted.

H58 on FAM126A likely forms a salt bridge with E761 on EFR3A, and therefore the mutant H58E was made to introduce a charge-charge repulsion between the two residues (figure 11). Although there was an observable 1.2-fold decrease in response in the mutant when compared to the wild type, there was no significant difference between the two ($P = 0.2021$).

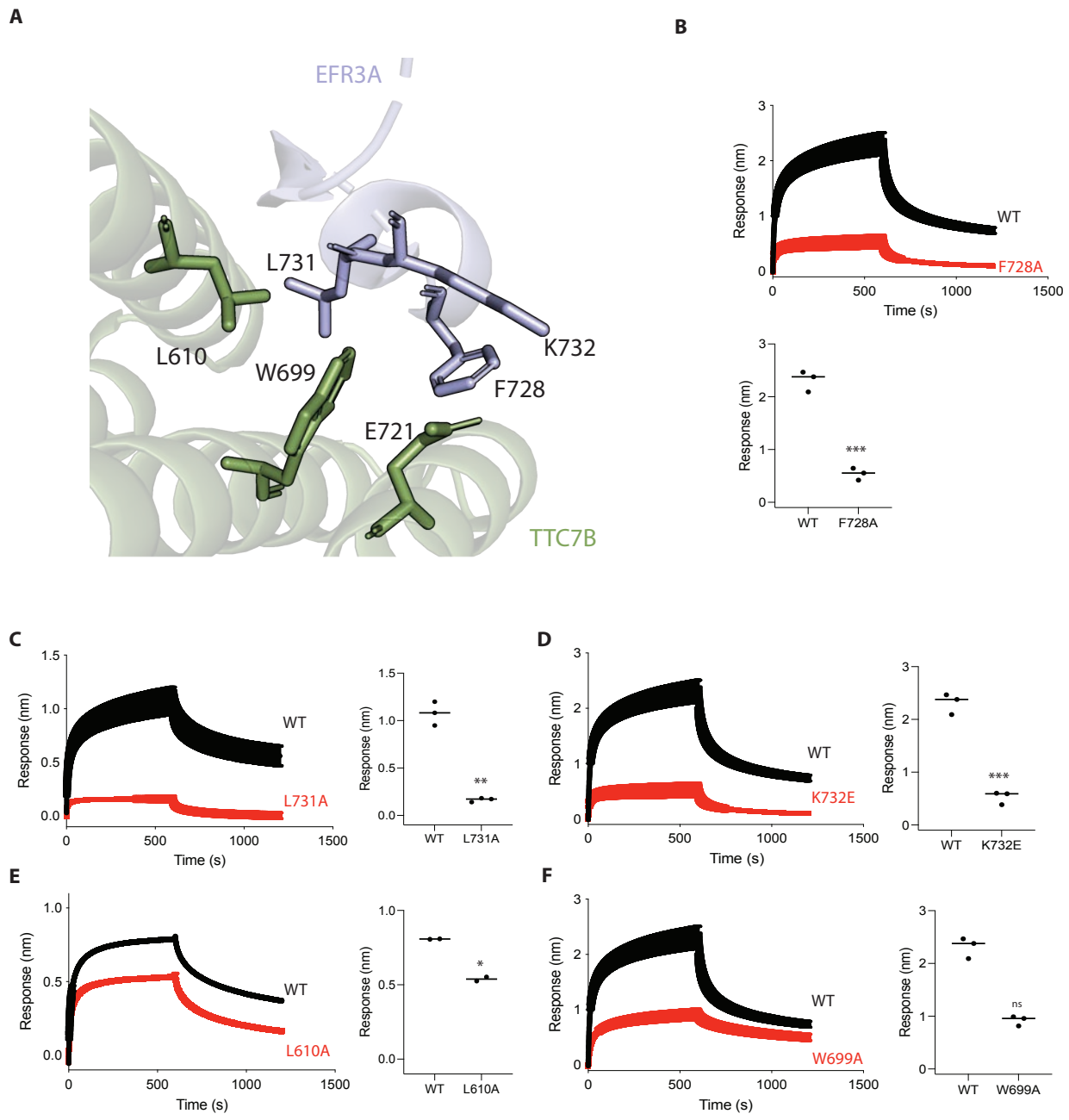

Figure 12. Mutations at the predicted EFR3A (721-791)/TTC7B interface disrupt binding. (A) A subsection of the predicted binding interface between EFR3A and TTC7B, generated using AlphaFold. (B-F) BLI measurements taken during association and dissociation of wild-type protein and the respective mutant. 200 nM EFR3A was loaded onto the optical fiber tip. TTC7B/FAM126A was tested at 500 nM. Mutants were statistically compared to wild-type binding using a two-tailed T-test with Welch's correction. ns = no significance, * = $P < 0.05$, ** = $P < 0.01$, *** = $P < 0.001$.

The residues F728 and L731 on EFR3A likely associate with TTC7B via hydrophobic residues L610 and W699; as shown in figure 12. The mutants F728A and L731A were generated to disrupt this binding niche. F728A had a significantly decreased response when compared to the wild type ($P = 0.0006$), as did L731A ($P = 0.0052$). A reciprocal experiment was performed with TTC7B mutants L610A and W699A. L610A had a significant effect on binding ($P = 0.0299$), with an observable 1.6-fold reduction in response when compared to the wild type. However, W699A did not have a significant effect on binding ($P = 0.3647$), even though there was an observed 2.5-fold decrease in response of the mutant compared to the wild type.

K732 on EFR3A likely forms a salt bridge with E721 on TTC7B, as such the mutant K732E was generated to introduce a charge-charge repulsion between the two residues (figure 12). The mutant had a significant effect on binding when compared to the wild type ($P = 0.0005$).

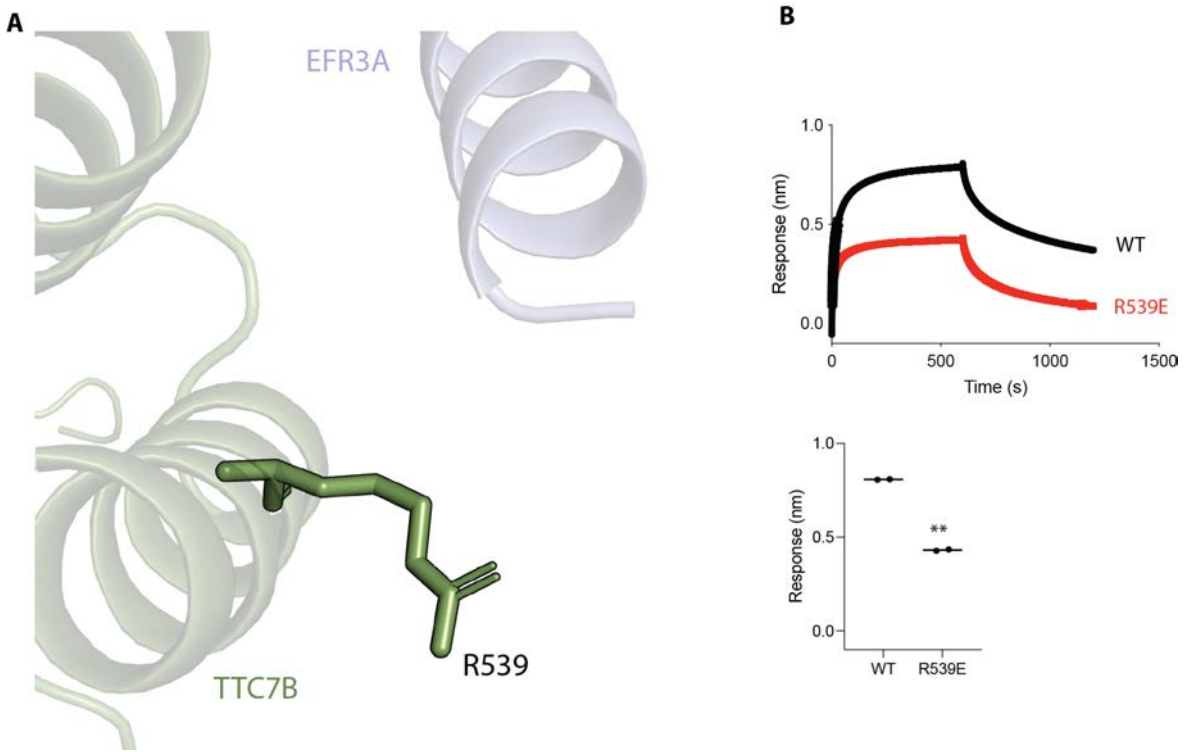

Figure 13. Mutations made at the predicted EFR3A (721-791)/TTC7B interface disrupt binding. (A) A subsection of the predicted binding interface between EFR3A and TTC7B, generated using AlphaFold. (B) BLI measurements taken during association and dissociation of wild type protein and the given mutant. 200 nM EFR3A was loaded onto the optical fiber tip. TTC7B/FAM126A was tested at 500 nM. The mutant was statistically compared to wild-type binding using a two-tailed T-test with Welch's correction. ** = $P < 0.01$.

Finally, the residue R539 likely associates with a negatively charged residue on EFR3A by forming a salt bridge (figure 13). Because of the low pLDDT score in the third helix of EFR3A in the AlphaFold model, a potential interaction partner for R539 could not be determined. Nevertheless, the mutant R539E was created with the intent of introducing a charge-charge repulsion to disrupt binding. The mutant exhibited a significant decrease in response when compared to the wild type ($P = 0.0022$). Taken together, these results support the model of the EFR3A (721-791)/TTC7B/FAM126A (2-308) binding complex predicted by AlphaFold.

Discussion

Production of PI4P by PI4KA is a fundamental part of signaling in eukaryotic cells (G. R. V. Hammond et al., 2012). Diseases associated with the dysregulation of PI4KA, including cancer and HCV, have profound impacts on the health of many individuals. For severe diseases such as cancer, there are only a handful of partially effective treatments available to those afflicted. This work provides additional insight into the interactions between TTC7B/FAM126A and EFR3A, and provides a molecular basis for the continued exploration of the role of the PI4KA regulatory complex in phosphoinositide metabolism and human disease.

PI4P is produced at the PM by phosphorylation of the 4′ position on the inositol headgroup of PI, which is catalyzed by the enzyme PI4KA. PI4P is an important precursor molecule for the production of PIP_2 and PIP_3, which both serve as signaling molecules in important pathways involving phospholipase C and Akt kinase, respectively (Dornan et al., 2018). Because of the importance of PI4P in cellular signaling, PI4KA activity and localization is tightly regulated. Accessory proteins TTC7B and FAM126A serve as scaffolds, and are essential for proper PI4KA functionality. The dimerization domain of PI4KA allows for the formation of a dimer of heterotrimers, resulting in the PI4KA regulatory complex (Lees et al., 2017). The putative mechanism of recruitment to the PM involves the membrane protein EFR3A, which recruits the regulatory complex to the PM through the association of its C-terminus with TTC7B and FAM126A (Wu et al., 2014). The interaction of EFR3A with the PI4KA regulatory complex promotes production of PI4P at the PM, allowing for downstream signaling (Dornan et al., 2018).

That being said, the exact mechanisms behind the recruitment of the PI4KA regulatory complex to the PM is not well understood at the molecular level. Published work has shown that

proper function of PI4KA is essential for survival. Inhibition of PI4KA is lethal in mouse models; furthermore, complete knockout of the PI4KA gene in mouse models also resulted in mortality (Bojjireddy et al., 2014). As mentioned, PI4KA is involved in cellular signaling pathways linked to numerous diseases. Investigation into the recruitment of the PI4KA regulatory complex may better our understanding of its regulation.

Previous work done by lab members had shown that the interaction between EFR3A and the PI4KA regulatory complex could be studied using only the TTC7B/FAM126A dimer. As such, a construct containing full length TTC7B and truncated FAM126A (2-308) was expressed in *E. coli* cells and purified using affinity chromatography. The C-terminus of EFR3A (721-791) was also cloned into a plasmid and prepared in a similar fashion (figures 8, 9, and 10).

The AlphaFold model generated by previous lab members revealed the predicted binding interface. Coupled with a thorough analysis of EFR3A, TTC7B, and FAM126A sequence homology, proteins containing single residue mutations along the putative binding interface were generated. Previous work done by current lab members determined the dissociation constant of wild type EFR3A and TTC7B/FAM126A to be about 300 nM, using 1:1, site specific binding between the ligand protein and the analyte (figure 5). The binding affinity of the mutants was tested using BLI, and compared to wild type protein tested under the same conditions using a two-tailed T-test. The generated mutations had varying success, with some completely interrupting binding and others having a minimal effect.

The most notable results were those generated from the EFR3A mutants F728A, L731A, K732E, and F755A, all of which demonstrated a significant reduction in response in comparison to the wild type ($p < 0.05$). The mutations F61A and L106F of FAM126A, and L610A of TTC7B also showed a significant reduction in response ($p < 0.05$). Given the biochemical

properties of the residues F728, L731, F755, F61, and L610, it is likely that these amino acids associate via hydrophobic interactions (figures 11, 12, and 13) Upon association with the binding partner, hydrophobic amino acids are buried inside the structure such that they are shielded from the solvent, increasing the free energy of the system. When the hydrophobicity of these residues is reduced, they are unable to interact with other hydrophobic residues to the same degree and the interaction is broken, which reduces the affinity (Baldwin & Rose, 2016). In contrast, the addition of a bulky side chain to L106 on FAM126A reduces binding affinity due to steric hindrance.

The lysine residue at position 732 on EFR3A is positively charged (figure 12). We postulate that it forms a salt bridge with E721 on TTC7B, which stabilizes the binding interface between EFR3A and TTC7B/FAM126A. The mutation K732E reverses the charge of the residue and introduces additional positive charge, interrupting hydrogen bonding and reducing binding affinity (Pylaeva et al., 2018). As such, the indicated residues play an important role in the interaction between EFR3A and TTC7B/FAM126A.

It is worth noting that some variability between different wild type preps of EFR3A were observed, which may be mitigating or intensifying the observed reduction in response when testing the mutants (figure 8, figure 9, figure A1, figure A2, figure A5). It is possible that a perceived significant difference in binding affinity may be due to variability of the wild type EFR3A, and further testing of variability between preps is needed.

Conclusions

EFR3A C-terminal constructs were designed and purified to test binding with the TTC7B/FAM126A dimer. Using the AlphaFold model as a guide, we identified the binding interface between these proteins, and used the model to predict which amino acids are likely involved in the interaction. Mutants of the amino acids within the binding region were made, and the affinity of the interaction was measured using biolayer interferometry (BLI). The dissociation constant (K_D) between EFR3A (721-791) and TTC7B/FAM126A (2-308) was measured at about 300 nM. The mutant proteins were compared to the wild type using BLI, and the experimental data from these assays was used to validate the AlphaFold model. This work details the structural basis behind the interaction of the EFR3A C-terminus with the TTC7B/FAM126A (2-308) dimer. Understanding the molecular mechanisms behind the recruitment of the PI4KA regulatory complex to the PM will further our understanding of its role in different signaling pathways. How these key amino acids along the binding interface lend themselves to the recruitment of the PI4KA regulatory complex to the PM remains unclear, and more work is required to fully understand this mechanism.

Future Directions

To further our understanding of the molecular mechanisms behind the PI4KA regulatory complex recruitment to the PM, we can continue our mutagenesis of the binding interface of EFR3A (721-791)/TTC7B/FAM126A (2-308) to validate the AlphaFold model. Work done by Baird et al., (2008) has shown that the yeast homologs of PI4KA and TTC7, Stt4 and Ypp1 respectively, along with EFR3, are essential for recruitment of PI4KA to the PM and production of PI4P there. To investigate recruitment of the PI4KA regulatory complex to the PM in mammalian cells, we can clone successful mutants (as determined by BLI) into mammalian vectors, and recruitment of the PI4KA complex can be studied in vivo using fluorescence microscopy. Ideally, this will confirm the effect of the mutation on PI4KA regulatory complex recruitment to the PM, and further our understanding of the molecular mechanisms behind its recruitment.

References

Adhikari, H., Kattan, W. E., Kumar, S., Zhou, P., Hancock, J. F., & Counter, C. M. (2021). Oncogenic KRAS is dependent upon an EFR3A-PI4KA signaling axis for potent tumorigenic activity. Nature Communications, 12(1), Article 1. https://doi.org/10.1038/s41467-021-25523-5

Baird, D., Stefan, C., Audhya, A., Weys, S., & Emr, S. D. (2008). Assembly of the PtdIns 4-kinase Stt4 complex at the plasma membrane requires Ypp1 and Efr3. The Journal of Cell Biology, 183(6), 1061–1074. https://doi.org/10.1083/jcb.200804003

Baldwin, R. L., & Rose, G. D. (2016). How the hydrophobic factor drives protein folding. Proceedings of the National Academy of Sciences, 113(44), 12462–12466. https://doi.org/10.1073/pnas.1610541113

Baskin, J. M., Wu, X., Christiano, R., Oh, M. S., Schauder, C. M., Gazzerro, E., Messa, M., Baldassari, S., Assereto, S., Biancheri, R., Zara, F., Minetti, C., Raimondi, A., Simons, M., Walther, T. C., Reinisch, K. M., & De Camilli, P. (2016). The leukodystrophy protein FAM126A (hyccin) regulates PtdIns(4)P synthesis at the plasma membrane. Nature Cell Biology, 18(1), Article 1. https://doi.org/10.1038/ncb3271

Bojjireddy, N., Botyanszki, J., Hammond, G., Creech, D., Peterson, R., Kemp, D. C., Snead, M., Brown, R., Morrison, A., Wilson, S., Harrison, S., Moore, C., & Balla, T. (2014). Pharmacological and Genetic Targeting of the PI4KA Enzyme Reveals Its Important Role in Maintaining Plasma Membrane Phosphatidylinositol 4-Phosphate and Phosphatidylinositol 4,5-Bisphosphate Levels. Journal of Biological Chemistry, 289(9), 6120–6132. https://doi.org/10.1074/jbc.M113.531426

Bojjireddy, N., Guzman-Hernandez, M. L., Reinhard, N. R., Jovic, M., & Balla, T. (2015). EFR3s are palmitoylated plasma membrane proteins that control responsiveness to G-protein-coupled receptors. Journal of Cell Science, 128(1), 118–128. https://doi.org/10.1242/jcs.157495

Boura, E., & Nencka, R. (2015). Phosphatidylinositol 4-kinases: Function, structure, and inhibition. Experimental Cell Research, 337(2), 136–145. https://doi.org/10.1016/j.yexcr.2015.03.028

Chang-Ileto, B., Frere, S. G., & Di Paolo, G. (2012). Acute Manipulation of Phosphoinositide Levels in Cells. Methods in Cell Biology, 108, 187–207. https://doi.org/10.1016/B978-0-12-386487-1.00010-9

Chung, J., Torta, F., Masai, K., Lucast, L., Czapla, H., Tanner, L. B., Narayanaswamy, P., Wenk, M. R., Nakatsu, F., & De Camilli, P. (2015). PI4P/phosphatidylserine countertransport at ORP5- and ORP8-mediated ER-plasma membrane contacts. Science, 349(6246), 428–432.

D'Angelo, G., Uemura, T., Chuang, C.-C., Polishchuk, E., Santoro, M., Ohvo-Rekilä, H., Sato, T., Di Tullio, G., Varriale, A., D'Auria, S., Daniele, T., Capuani, F., Johannes, L., Mattjus, P., Monti, M., Pucci, P., Williams, R. L., Burke, J. E., Platt, F. M., … De Matteis, M. A. (2013). Vesicular and non-vesicular transport feed distinct glycosylation pathways in the Golgi. Nature, 501(7465), 116–120. https://doi.org/10.1038/nature12423

Di Paolo, G., & De Camilli, P. (2006). Phosphoinositides in cell regulation and membrane dynamics. Nature, 443(7112), 651–657. https://doi.org/10.1038/nature05185

Dornan, G. L., Dalwadi, U., Hamelin, D. J., Hoffmann, R. M., Yip, C. K., & Burke, J. E. (2018a). Probing the Architecture, Dynamics, and Inhibition of the PI4KIIIα/TTC7/FAM126 Complex. Journal of Molecular Biology, 430(18, Part B), 3129–3142. https://doi.org/10.1016/j.jmb.2018.07.020

Dornan, G. L., Dalwadi, U., Hamelin, D. J., Hoffmann, R. M., Yip, C. K., & Burke, J. E. (2018b). Probing the Architecture, Dynamics, and Inhibition of the PI4KIIIα/TTC7/FAM126 Complex. Journal of Molecular Biology, 430(18, Part B), 3129–3142. https://doi.org/10.1016/j.jmb.2018.07.020

Hammond, G. R., & Burke, J. E. (2020). Novel roles of phosphoinositides in signaling, lipid transport, and disease. Current Opinion in Cell Biology, 63, 57–67. https://doi.org/10.1016/j.ceb.2019.12.007

Hammond, G. R. V., Fischer, M. J., Anderson, K. E., Holdich, J., Koteci, A., Balla, T., & Irvine, R. F. (2012). PI4P and PI(4,5)P2 Are Essential But Independent Lipid Determinants of Membrane Identity. Science, 337(6095), 727–730. https://doi.org/10.1126/science.1222483

Hemmings, B. A., & Restuccia, D. F. (2012). PI3K-PKB/Akt Pathway. Cold Spring Harbor Perspectives in Biology, 4(9), a011189. https://doi.org/10.1101/cshperspect.a011189

Jumper, J., Evans, R., Pritzel, A., Green, T., Figurnov, M., Ronneberger, O., Tunyasuvunakool, K., Bates, R., Žídek, A., Potapenko, A., Bridgland, A., Meyer, C., Kohl, S. A. A., Ballard, A. J., Cowie, A., Romera-Paredes, B., Nikolov, S., Jain, R., Adler, J., … Hassabis, D. (2021). Highly accurate protein structure prediction with AlphaFold. Nature, 596(7873), Article 7873. https://doi.org/10.1038/s41586-021-03819-2

Lees, J. A., Zhang, Y., Oh, M. S., Schauder, C. M., Yu, X., Baskin, J. M., Dobbs, K., Notarangelo, L. D., De Camilli, P., Walz, T., & Reinisch, K. M. (2017). Architecture of the human PI4KIIIα lipid kinase complex. Proceedings of the National Academy of Sciences, 114(52), 13720–13725. https://doi.org/10.1073/pnas.1718471115

Li, J., Wang, X., Zhang, T., Wang, C., Huang, Z., Luo, X., & Deng, Y. (2015). A review on phospholipids and their main applications in drug delivery systems. Asian Journal of Pharmaceutical Sciences, 10(2), 81–98. https://doi.org/10.1016/j.ajps.2014.09.004

Lim, Y.-S., & Hwang, S. B. (2011). Hepatitis C Virus NS5A Protein Interacts with Phosphatidylinositol 4-Kinase Type IIIα and Regulates Viral Propagation*. Journal of Biological Chemistry, 286(13), 11290–11298. https://doi.org/10.1074/jbc.M110.194472

McPhail, J. A., & Burke, J. E. (2022). Molecular mechanisms of PI4K regulation and their involvement in viral replication. Traffic, 24(3). https://doi.org/10.1111/tra.12841

Mesmin, B., Bigay, J., Polidori, J., Jamecna, D., Lacas-Gervais, S., & Antonny, B. (2017). Sterol transfer, PI4P consumption, and control of membrane lipid order by endogenous OSBP. The EMBO Journal, 36(21), 3156–3174. https://doi.org/10.15252/embj.201796687

Mo, S. P., Coulson, J. M., & Prior, I. A. (2018). RAS variant signalling. Biochemical Society Transactions, 46(5), 1325–1332. https://doi.org/10.1042/BST20180173

Nakatsu, F., Baskin, J. M., Chung, J., Tanner, L. B., Shui, G., Lee, S. Y., Pirruccello, M., Hao, M., Ingolia, N. T., Wenk, M. R., & De Camilli, P. (2012). PtdIns4P synthesis by PI4KIIIα at the plasma membrane and its impact on plasma membrane identity. The Journal of Cell Biology, 199(6), 1003–1016. https://doi.org/10.1083/jcb.201206095

Orthwein, T., Huergo, L. F., Forchhammer, K., & Selim, K. A. (2021). Kinetic Analysis of a Protein-protein Complex to Determine its Dissociation Constant (KD) and the Effective Concentration (EC50) of an Interplaying Effector Molecule Using Bio-layer Interferometry. Bio-Protocol, 11(17), e4152. https://doi.org/10.21769/BioProtoc.4152

Prior, I. A., Hood, F. E., & Hartley, J. L. (2020). The Frequency of Ras Mutations in Cancer. Cancer Research, 80(14), 2969–2974. https://doi.org/10.1158/0008-5472.CAN-19-3682

van Meer, G., Voelker, D. R., & Feigenson, G. W. (2008). Membrane lipids: Where they are and how they behave. Nature Reviews Molecular Cell Biology, 9(2), 112–124. https://doi.org/10.1038/nrm2330

Varadi, M., Anyango, S., Deshpande, M., Nair, S., Natassia, C., Yordanova, G., Yuan, D., Stroe, O., Wood, G., Laydon, A., Žídek, A., Green, T., Tunyasuvunakool, K., Petersen, S., Jumper, J., Clancy, E., Green, R., Vora, A., Lutfi, M., … Velankar, S. (2022). AlphaFold Protein Structure Database: Massively expanding the structural coverage of protein-sequence space with high-accuracy models. Nucleic Acids Research, 50(D1), D439–D444. https://doi.org/10.1093/nar/gkab1061

Wu, X., Chi, R. J., Baskin, J. M., Lucast, L., Burd, C. G., De Camilli, P., & Reinisch, K. M. (2014). Structural insights into assembly and regulation of the plasma membrane phosphatidylinositol 4-kinase complex. Developmental Cell, 28(1), 19–29. https://doi.org/10.1016/j.devcel.2013.11.012

Appendix

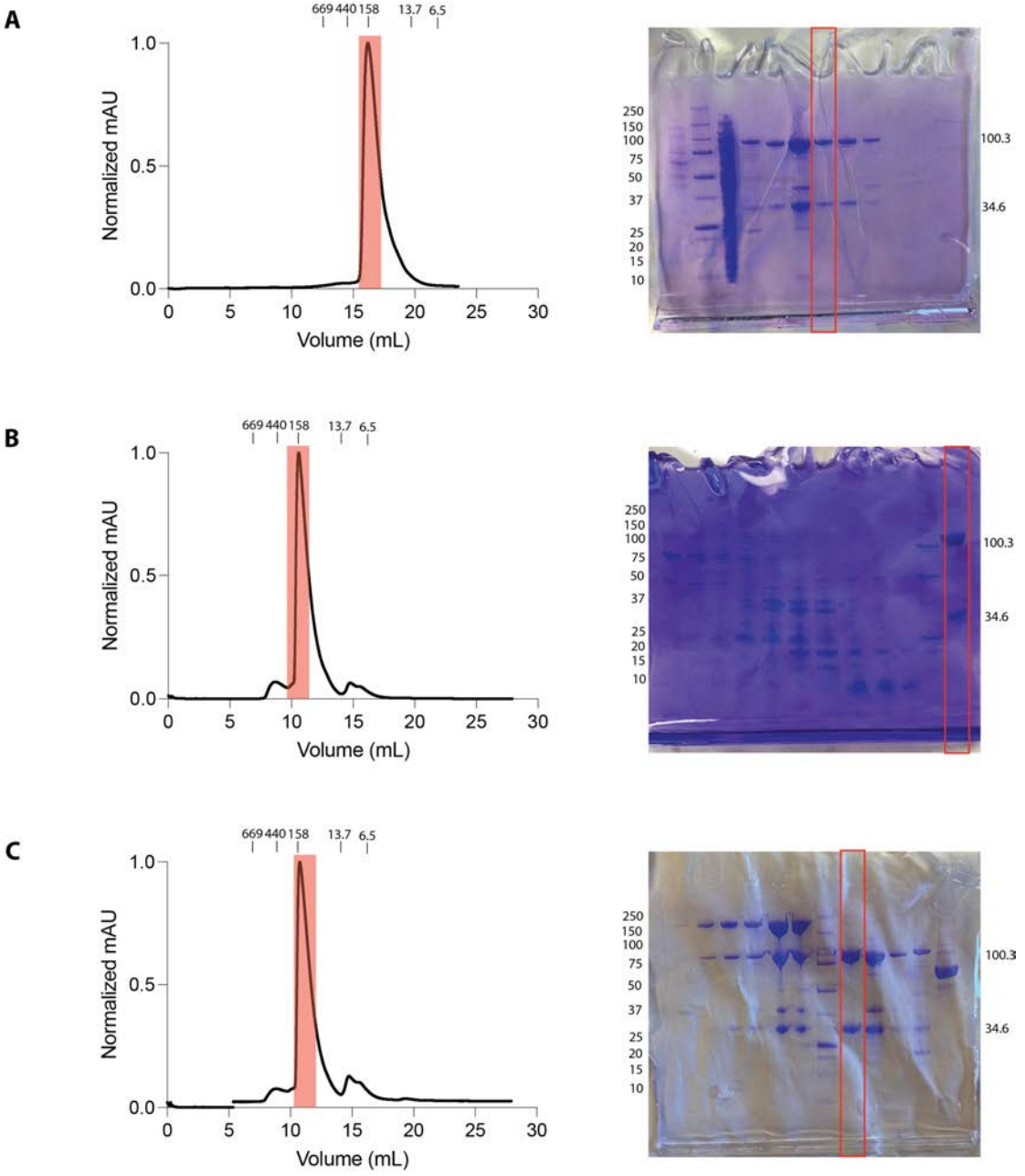

Figure A1. Purification of TTC7B/FAM126A (full-length TTC7B, FAM126A 2-308) mutants W699A, L610A, and R539E. Red boxes indicate fractions taken, which were run on the adjacent uncropped SDS-PAGE gel, stained with Coomassie blue and run at 200 V for 30 minutes. (A) Size exclusion chromatography trace of W699A TTC7B/FAM126A mutant, run on a Superose 6 Increase 10/300 GL size exclusion column. (B) Purification of L610A TTC7B/FAM126A mutant, run on a Superdex 200 Increase 10/300 GL size exclusion column. (C) Purification of R539E TTC7B/FAM126A mutant, run on a Superdex 200 Increase 10/300 GL size exclusion column.

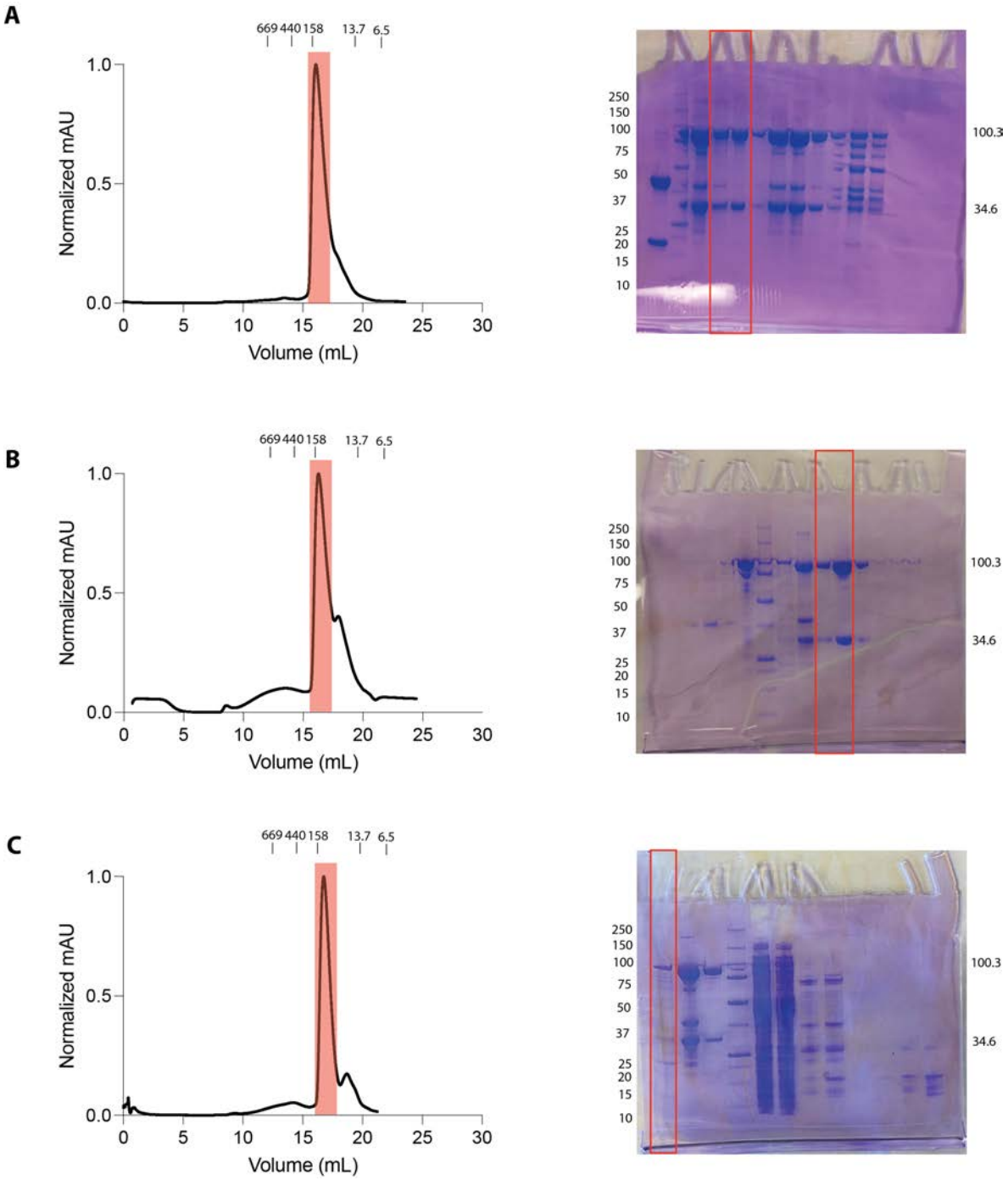

Figure A2. Purification of TTC7B/FAM126A (full-length TTC7B, FAM126A 2-308) mutants L106F, H58E, and F61A. Red boxes indicate fractions taken, which were run on the adjacent uncropped SDS-PAGE gel, stained with Coomassie blue and run at 200 V for 30 minutes. (A) Size exclusion chromatography trace of L106F TTC7B/FAM126A mutant, run on a Superose 6 Increase 10/300 GL size exclusion column. (B) Purification of H58E TTC7B/FAM126A mutant, run on a Superose 6 Increase 10/300 GL GL size exclusion column. (C) Purification of F61A TTC7B/FAM126A mutant, run on a Superose 6 Increase 10/300 GL size exclusion column.

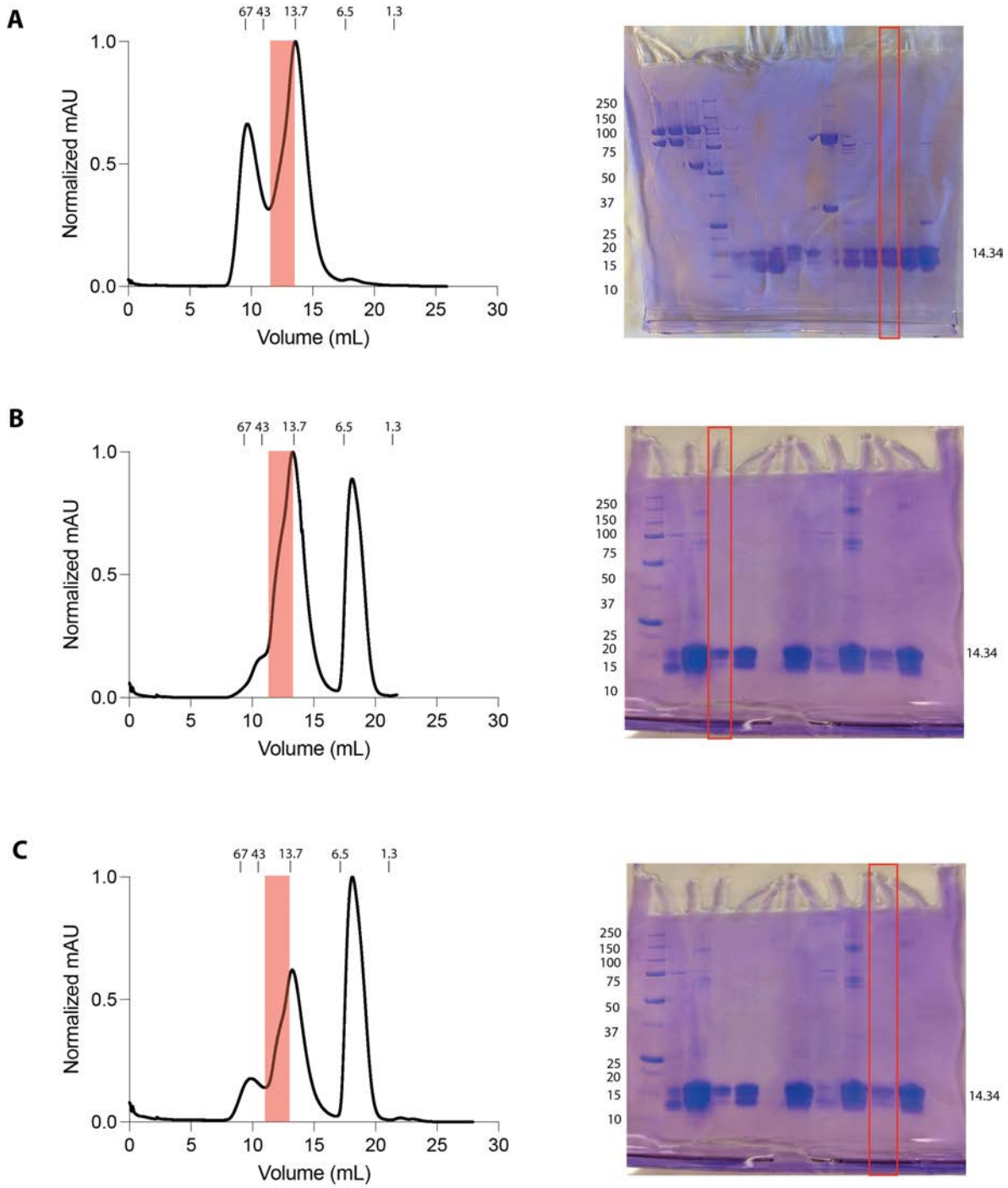

Figure A3. Purification of EFR3A (721-791) mutants L731A, F728A, and K732E. Red boxes indicate fractions taken, which were run on the adjacent uncropped SDS-PAGE gel, stained with Coomassie blue and run at 200 V for 30 minutes. (A) Size exclusion chromatography trace of L731A EFR3A mutant, run on a S75 Increase 10/300 GL size exclusion column. (B) Purification of F728A EFR3A mutant, run on a S75 Increase 10/300 GL size exclusion column. (C) Purification of K732E EFR3A mutant, run on a S75 Increase 10/300 GL size exclusion column.

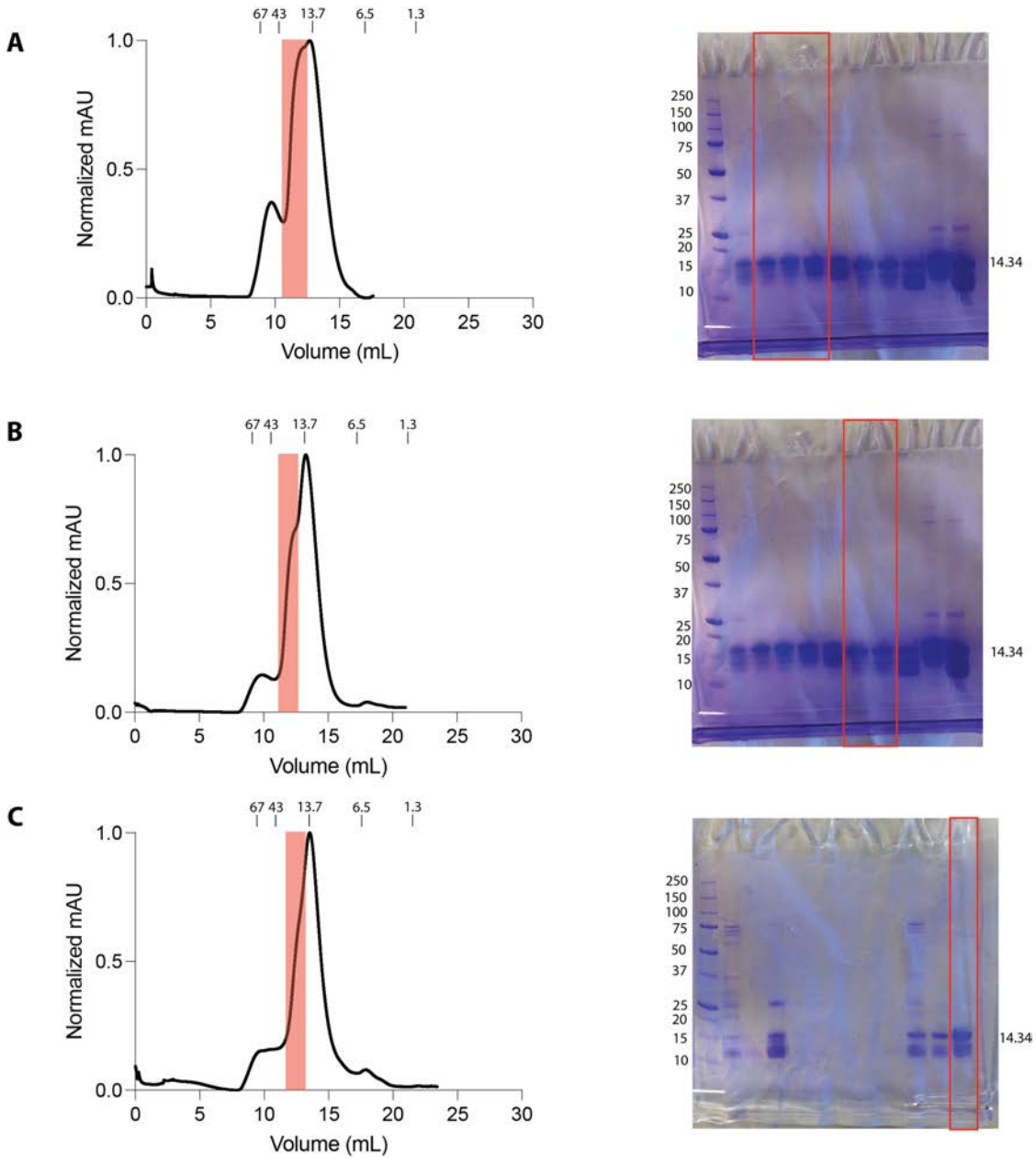

Figure A4. Purification of EFR3A (721-791) mutants F760A, F755A, and I763A. Red boxes indicate fractions taken, which were run on the adjacent uncropped SDS-PAGE gel, stained with Coomassie blue and run at 200 V for 30 minutes. (A) Size exclusion chromatography trace of F760A EFR3A mutant, run on a S75 Increase 10/300 GL size exclusion column. (B) Purification of F755A EFR3A mutant, run on a S75 Increase 10/300 GL size exclusion column. (C) Purification of I763A EFR3A mutant, run on a S75 Increase 10/300 GL size exclusion column.

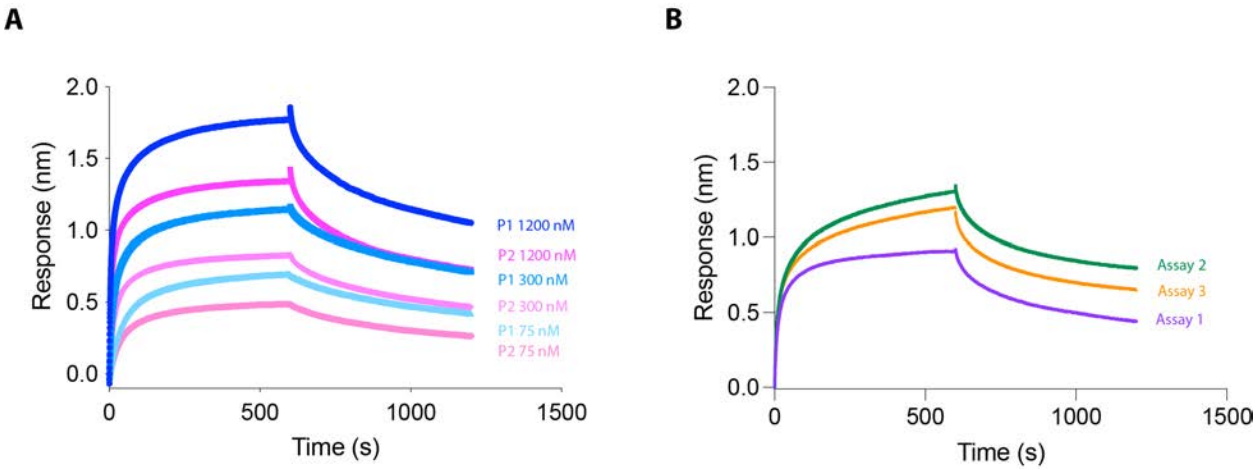

Figure A5. Determining reproducibility of wild type EFR3A (721-791) preps. (A) Dose-response of wild type EFR3A prep 1 and 2. Binding was assessed using 1200 nM, 300 nM, and 75 nM of TTC7B/FAM126A. (B) Response of wild type EFR3A prep 2 across multiple assays. Binding was assessed using 500 nM of TTC7B/FAM126A dimer.